13

UCRL 8423

UNIVERSITY OF
CALIFORNIA

Radiation Laboratory

NUCLEAR DECAY STUDIES OF PROTACTINIUM ISOTOPES

BERKELEY, CALIFORNIA

DISCLAIMER

UCRL-8423

UNIVERSITY OF CALIFORNIA
Radiation Laboratory
Berkeley, California

Contract No. W-7405-eng-48

NUCLEAR DECAY STUDIES OF PROTACTINIUM ISOTOPES

Max W. Hill

(Thesis)

August 1958

Printed for the U. S. Atomic Energy Commission

NUCLEAR DECAY STUDIES OF PROTACTINIUM ISOTOPES

Contents

NUCLEAR DECAY STUDIES OF PROTACTINIUM ISOTOPES

Max W. Hill

Radiation Laboratory and Department of Chemistry
University of California, Berkeley, California

August 1958

ABSTRACT

A study was made of the radiations of the protactinium isotopes Pa^{227}, Pa^{228}, Pa^{229}, Pa^{230}, Pa^{232}, and Pa^{233}, as well as Ac^{223} and Ac^{224}, with primary emphasis placed on the investigation of the alpha-decay spectra with high-resolution alpha-particle spectrographs. Decay schemes are presented in each case, and are interpreted wherever possible in terms of current theoretical nuclear models. The collective model of Bohr and Mottelson finds wide application in most cases, although the complexity of the decay schemes leaves certain features unexplained.

NUCLEAR DECAY STUDIES OF PROTACTINIUM ISOTOPES

I. INTRODUCTION

Our knowledge and understanding of nuclear decay processes and nuclear structure have been greatly enhanced during the past few years by improved experimental techniques. Especially important has been the development and perfection of high-resolution nuclear spectroscopy, which has revealed a vast amount of information concerning nuclear states and their various properties, such as spin, parity, energy, etc. In an attempt to consolidate the fundamental concepts involved and successfully account for these nuclear properties, several nuclear models have been proposed, some of which have achieved remarkable success. The two models currently holding greatest promise are the single-particle shell model originally proposed by Mayer[1] and Jensen,[2] and the "strong-coupling" collective model of Bohr and Mottelson.[3] However, it has become increasingly apparent that there are special domains or regions throughout the periodic system where each of these models enjoys its greatest success, and others where neither may be applied satisfactorily. It is in these latter regions where the need for detailed knowledge of nuclear states is in greatest demand in order that theoretical contributions may be successfully advanced. The present study is directed toward the accumulation of new information and a better understanding of nuclides in such a region.

It now appears that there are at least three distinct regions in the domain of the heavy elements (beyond lead in the periodic table), each characterized by a different pattern of excited states and for which different nuclear models are appropriate. Near the doubly closed shell of Pb^{208} and extending only a few nucleons away, the spherical-well shell model has been successfully applied by Pryce[4] and True.[5] For the heaviest elements, with $N > 138$, a stabilized spheroidal deformation has set in, and the Bohr-Mottelson collective model has found great success. In the region lying beyond these two, much less is known, although models have been advanced by Goldhaber and Weneser[6] and Wilets and Jean[7] for

even-even nuclei with atomic number between about 86 and 88. The great complexity of levels in the odd-mass nuclides of this region has also been noted.[8]

Since the isotopes of protactinium lie on the very fringe of the collective-model region and seem to exhibit a great degree of complexity in their decay schemes, this study was undertaken to help further our understanding of this region. Primary emphasis was placed on the application of high-resolution alpha spectroscopy to study the alpha groups of Pa^{227}, Pa^{228}, and Pa^{229}, the fine structure of which had never been observed. In the course of the study the electron-capture and beta decays of these and other isotopes of protactinium were also examined, and the results are included. Interest in the decay of protactinium isotopes is also prompted by the fact that they are all of the odd-even or odd-odd type, of which much less is known than of even-even nuclides, and because beta and gamma vibrational states have appeared in this region, as well as very low-lying 1- states.

II. EXPERIMENTAL METHODS

In a nuclear decay study of protactinium isotopes, all the more common modes of decay are represented, including alpha-particle emission, electron capture, beta emission, and positron emission, each followed by internal transitions involving gamma rays and internal-conversion electrons. In order to effectively study these radiations, essentially all types of spectroscopic techniques and equipment could be used to advantage. In this study, recourse has been made to the three general types of nuclear spectroscopy — alpha, electron, and gamma. The alpha spectra were studied with high-resolution electromagnetic alpha-particle spectrographs. The electron studies were limited to conversion electrons from internal transitions and were made by employing photographic-recording permanent-magnet spectrographs. The gamma-ray studies were carried out with the aid of scintillation spectrometers, some of which were equipped for coincidence measurements. Details of each of these instruments are given in the following section, along with the methods of preparing and purifying the active materials used in this study.

A. Alpha Spectroscopy

1. Uniform-Field Alpha-Particle Spectrograph

The first alpha-particle spectrograph used in this study was the uniform-field or so-called "low geometry" spectrograph. It has been described in detail in the literature,[9] but the most important features are reviewed here. It is a converted Nier-type mass spectrograph employing a uniform-field 60°-sector electromagnet with a 1-inch gap between the pole pieces. The radius of curvature of the normal trajectory is 75 cm.

The magnet power supply on the spectrograph is capable of maintaining the current constant to one part in 10,000 over a 24-hour period. The current is monitored constantly with a recorder to detect current fluctuations. The magnetic field is measured by a proton fluxmeter, and is usually maintained in the 4-to-5-kilogauss region. The entire spectrograph is maintained at an operating vacuum of about 10^{-5} mm of mercury.

Figure 1 is a schematic drawing of the spectrograph, showing the relative positions of the source, baffles, magnet, and detector. The alpha-emitting source is placed behind a system of vertical defining slits some 50 inches from the magnet. Various combinations of defining slits, 1 inch in length and 0.001 to 0.125 inch in width, are used, depending upon the nature of the experiment. The beam is further defined by a pair of adjustable baffles just before the magnet. The different slit arrangements, together with the adjustable baffle system, allow a variation in transmission of from 10^{-4} to 10^{-7} of 4π.

After passing through the magnetic field, the focused beam of alpha particles impinges on a photographic plate placed at an angle of 30° to the path of the beam. The photographic plates are 9-by-2-inch Eastman NTA plates, with emulsions 25 microns thick. With the plate set at an angle of 30°, the alpha particles enter the emulsion at a 30° angle rather than perpendicular to it, leaving a track approximately 20 microns in length. Owing to the small angle of acceptance in the vertical direction permitted by the pole-tip gap, the alpha tracks on the plate should be very nearly parallel.

The developed emulsions are examined under a 450-power microscope with bright-field illumination. The alpha tracks are counted individually, and only those tracks which are parallel and of the right length are recorded. This allows a partial discrimination against background tracks, many of which originate from the inside surfaces of the main vacuum tank of the spectrograph (due to radioactive recoil nuclei emitted from the source) and in general strike the plate randomly.

The plate is placed horizontally on the microscope stage and the tracks are totaled for a vertical scan across the short dimension of the plate. Since the microscope field of view is 1/4 by 1/4 mm, a complete counting of the plate consists of making these scans every 1/4 mm across the length of the plate. The number of tracks observed in each vertical scan across the plate is then plotted against the position of the scan in the horizontal direction to give the alpha-particle spectrum. The position in the horizontal direction is converted to an energy scale by calibrating against known standards. In this work the standards most commonly used were $U^{230}_{\alpha_o}$ = 5.884 Mev and $Ra^{224}_{\alpha_o}$ = 5.681 Mev.

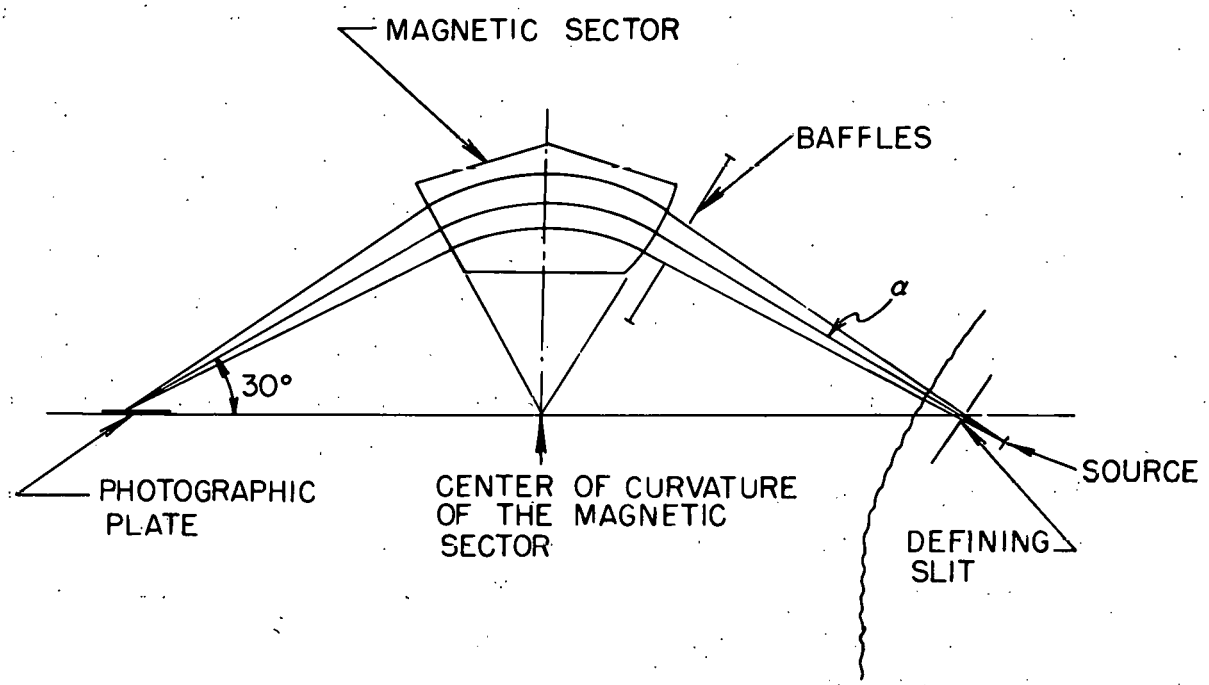

Fig. 1. Schematic diagram of uniform-field alpha-particle spectrograph.

The resolution of the spectrograph depends very strongly upon the thickness of the sample and upon the slit and baffle conditions employed. Under ordinary operating conditions, with an 0.018-inch defining slit and 3-inch baffle opening, a thin sample produces peaks with widths at half maximum of approximately 6 kev in 6 Mev of alpha-particle energy, or a resolution of 0.1%. By use of more stringent conditions peak widths of 1.4 kev have recently been obtained,[10] corresponding to a resolution of 0.023%.

In order to find the separation between peaks, the positions were taken as the midpoints of the peaks at half-maximum intensity. This has been shown to be more accurate and reliable than taking the high-energy edges as the peak positions. The distance between peaks is then multiplied by the dispersion in kev/mm to give the energy separation. The dispersion has been shown to be constant within 1% over the entire length of the plate, and is known roughly as a function of field strength. However, whenever possible the dispersion is determined experimentally by measuring the separation between alpha groups of known energy. For field strengths required to focus alpha particles of from 5 to 6.5 Mev, the dispersion is of the order of 3.2 to 4.2 kev/mm. This allows alpha groups differing in energy by 700 to 900 kev to be focused simultaneously at the extreme ends of one plate.

Extreme care must be taken in the preparation of the source for high-resolution alpha spectroscopy. Even the smallest amounts of material result in broadening of the peaks and in pronounced low-energy tailing due to energy degradation of the beam. Sources prepared by simple evaporation of a solution of the active material are especially unsuitable. A better method consists of electrodeposition of the active material onto the source holder. However, even with improved electrodeposition techniques, this method has failed to meet the standards required for a good source. The most generally acceptable method employed in this laboratory is vacuum sublimation. In this method, the material to be investigated is first purified from other activities by some procedure which introduces as little as possible extraneous mass. When the activity is radiochemically pure and as free from stray mass as possible, it is evaporated from

a hydrochloric or nitric acid solution onto a trough-shaped tungsten filament. The filament is shaped into a trough approximately 1/2 inch long and 0.04 inch deep by heating it in a specially prepared die. The system (enclosed by a bell jar) is evacuated to a pressure of less than a micron of mercury and the filament is preflashed at a dull-red heat to remove any volatile impurities. A plate, generally of 0.002-inch platinum, aluminum, or nickel, is then placed a short distance above the filament, and after re-evacuation, the activity is sublimed at white heat from the filament onto the cool plate. The sample thus obtained is generally quite thin and uniform, and may be restricted to a very small area. Further purification both from radioactive impurities and from extraneous mass is made possible by subliming only over a narrow range of temperature. In this study, the range of temperature over which protactinium sublimes was determined beforehand, and carefully controlled during subsequent sublimations. It was found that protactinium sublimed at a relatively low temperature and could be separated from less volatile activities such as zirconium, which is one of its more troublesome contaminants, by keeping the temperature relatively low.

2. Double-Focusing Alpha-Particle Spectrograph

Most of the alpha-particle spectra obtained during the course of this study were taken with the newer double-focusing alpha-particle spectrograph. The principal advantage of this instrument is its much higher transmission — a factor about 10 higher than that of the uniform-field spectrograph — with little, if any, decrease in resolution. The magnet covers 180° with a maximum radius of 50 cm, and a normal radius of 35 cm. The field is nonuniform, being chosen with a radial dependence which produces focusing in both vertical and horizontal directions. Fields of 8 to 14 kilogauss at the normal radius are employed.

Figure 2 is a schematic drawing of the spectrograph showing the relative positions of the source, defining slits, baffles, magnet, and coincidence detector. For taking straight alpha-particle spectra, the zinc sulfide screen assembly is replaced by a photographic plate holder similar to that used in the uniform-field spectrograph, and the spectra

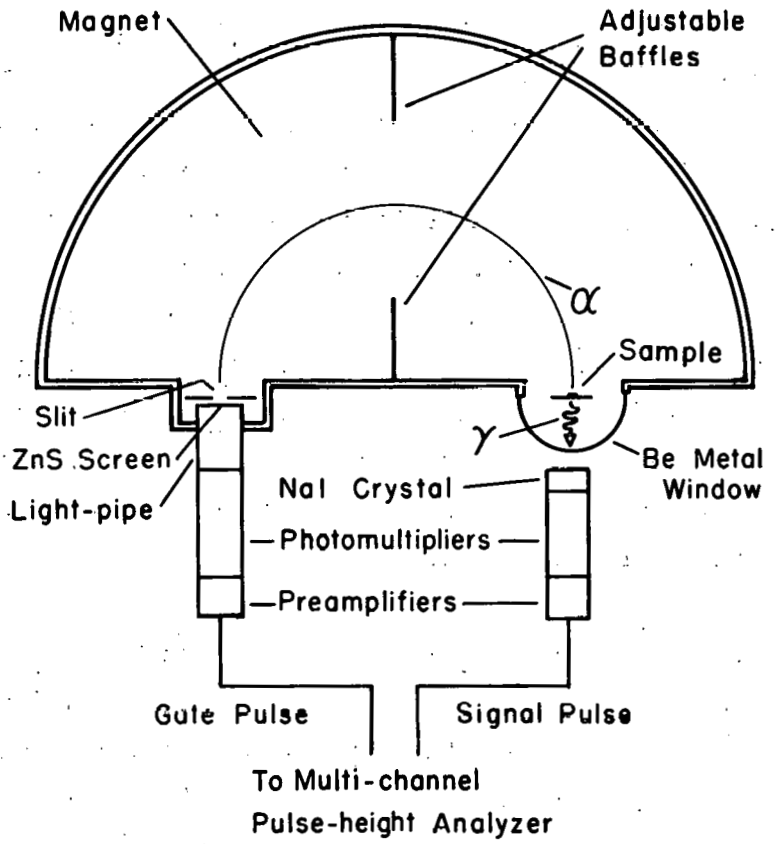

Fig. 2. Schematic diagram of double-focusing alpha-particle spectrograph arranged for alpha-gamma coincidence studies.

recorded in much the same way. The plates for this holder measure 1-15/64 by 9 inches.

The magnet-current supply and vacuum systems have been designed to give the same performance as those of the older instrument. The field is measured in terms of the frequency of the nuclear magnetic resonance of Li^7.

Because of the variation in field, the dispersion varies markedly over the length of the plate, and is thus a function of position as well as field strength. In order to determine the energy separations of alpha groups, calibration curves have been obtained with standard alpha emitters, and the following equation developed:

$$\frac{E\ (kev)}{H^2} = 14.0486 - 0.0091330X + Y_X . \qquad (1)$$

Here X is the position of the peak on the photographic plate (in mm from the high-energy end of the plate), H is the effective magnetic field (in megacycles), and Y_X is a correction term depending upon the position of the peak on the photographic plate. (Fig. 3). The effective magnetic field is best determined by the position of a standard peak, although curves for relating the observed magnetic field as determined by the Li^7 resonance frequency to the effective magnetic field have also been developed.[8] Use of this equation enables energy separations and absolute energies to be calculated with a knowledge of H and X.

The variation in field also markedly affects the quality of the peaks; those toward either end of the plate are broadened and distorted. Figure 4 shows the spectrum obtained by focusing the alpha groups of Cf^{250} and Cf^{252} at five different positions on the same photographic plate. The distortion is especially pronounced at both ends of the plate. This spectrum was obtained by using a 0.020-inch defining slit and 3.0-cm baffle openings. At larger baffle openings the distortion is even more pronounced, while at smaller baffle openings the quality of the peaks is somewhat improved. Investigations are currently being carried out to ascertain the effects of baffle opening, slit width, and position upon the shapes of standard peaks.[10]

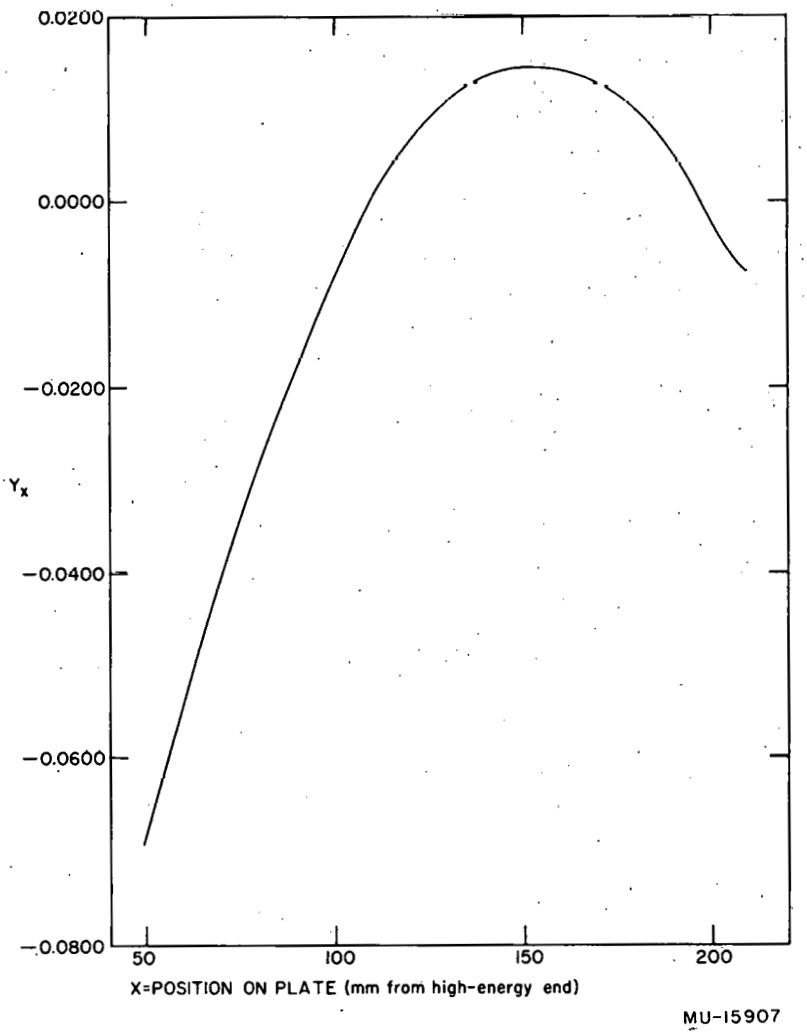

Fig. 3. Calibration curve for double-focusing alpha-particle spectrograph.

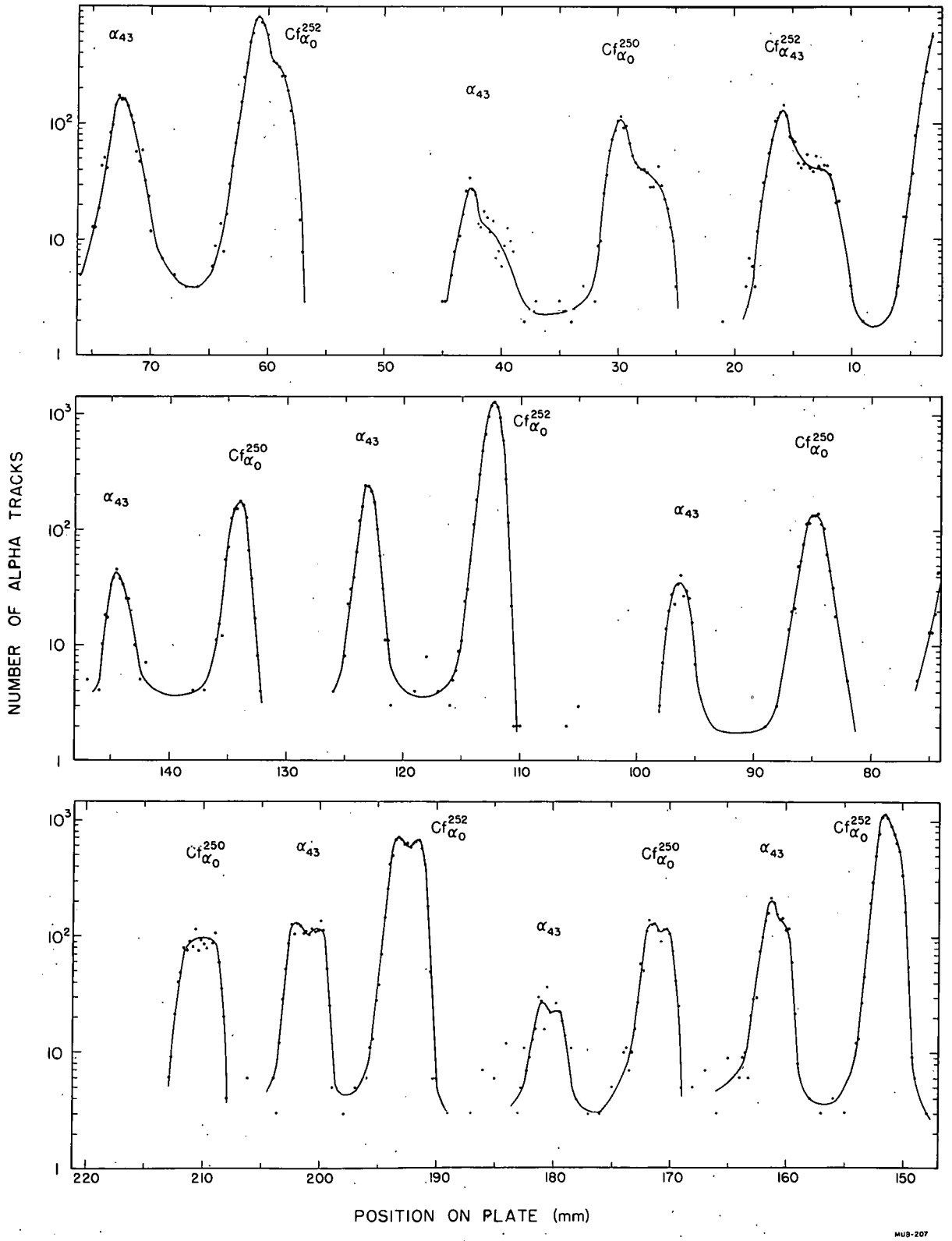

Fig. 4. Alpha groups of Cf^{250} and Cf^{252}, showing variation of peak shape with position on plate — double-focusing spectrograph.

Previous investigations had indicated that the relative transmission of the spectrograph was a function of the position of a peak on the photographic plate and tended to fall off slightly at lower positions.[8] In order to check this, the alpha particles from Cf^{250} and Cf^{252} were allowed to strike a photographic plate for a given period of time at different field settings (Fig. 4). If the transmission were the same for all positions, the number of tracks recorded should be the same for each field setting, regardless of the positions of the peaks. Table I lists the numbers of tracks recorded for three different field settings for four different experiments. The numbers in parenthesis are the same figures normalized so that the number of tracks in the center portion of the plate is the same for each experiment. It can be seen from the table that there is no trend toward lower transmission at any position on the plate. The standard deviation of 1.6% is certainly no larger than the combined statistical (1.0% for 10,000 tracks) and track counting errors. Similar results are obtained by integrating the four $Cf^{252}_{\alpha_o}$ peaks shown in the spectrum of Fig. 4. The numbers of tracks under the peaks at 61, 112, 151, and 192 mm are 8241, 8421, 8350, and 8503 respectively. The average with its standard deviation is 8379 ± 96. Again, the deviation is easily accounted for by statistical and counting errors.

Table I. Relative transmission of double-focusing alpha-particle spectrograph (normalized values in parenthesis)

Experiment number	Number of alpha tracks Region of plate		
	Lower	Center	Upper
202	11393 (9963)	11435 (10000)	11539 (10091)
203	11650 (10276)	11337 (10000)	11180 (9862)
204	9574 (9858)	9712 (10000)	9956 (10251)
205	9984 (10272)	9720 (10000)	10003 (10335)
Average: 10076 ± 160			

Since the alpha particles are focused both vertically and horizontally by the magnetic field, the alpha tracks recorded on the photographic plate give a virtual image of the alpha-emitting source. If the source is not placed in a precisely vertical position, the alpha tracks will not fall along a vertical line. In this case the scan across the plate must be made at a slight angle to the vertical for maximum resolution. This angle is determined experimentally by drawing a thin horizontal line along the length of the plate and separately recording the numbers of tracks on the upper and lower portions for a given angle. If the proper angle is chosen, the number of tracks in each portion will reach a maximum at the same position. If the angle is improperly chosen, the maximum for one portion will be reached at a slightly different position from the maximum for the other portion. In this work the proper angle for each different source was determined by counting over one peak in this manner before proceeding to the entire spectrum.

The high transmission of this instrument permits alpha-particle–gamma-ray coincidence studies to be made where coincidences with a particular alpha group are desired. The photographic plate is replaced with a zinc sulfide screen masked except for a narrow vertical slit and coupled through a light type to a photomultiplier tube. The magnetic field is adjusted to focus a particular alpha group on the slit and the scintillations caused by the alpha particles striking the ZnS screen are counted and fed into a coincidence circuit to serve as gate pulses. The source holder has been constructed with a beryllium window to permit low-energy gamma rays emitted by the source to be detected by an external sodium iodide scintillation spectrometer (see Fig. 3). Coincidences can then be run between gamma rays and alpha particles of a given energy. The spectrum is displayed on a 100-channel pulse-height analyzer. This method was attempted in the alpha decay of Pa^{229}, but yielded little information because of the small ratio of alpha to beta-gamma activity of the sample, coupled with instrument difficulties.

Additional information may be obtained by varying the position of the gamma detector and thus obtaining the angular distribution of gamma rays with respect to the given alpha group. This type of experiment was not undertaken in this study.

B. Electron Spectroscopy

The conversion-electron spectra were recorded with the aid of photographic-recording uniform-field permanent-magnet spectrographs (see Fig. 5). The source consists of a platinum wire of 0.010-inch diameter on which the active material is electrodeposited. The design is such that the wire is located in a readily reproducible position in the spectrograph. The electrons are collimated by a permanently fixed defining slit, and after being bent and focused by the magnetic field are allowed to strike a 25 micron thick no-screen X-ray emulsion plate, producing visible lines. Both source and detector are located inside the magnetic field.

From its position on the plate, the energy of an electron line is calculated by use of calibration curves developed by W. G. Smith and J. M. Hollander for each particular instrument.[11] In this study, calibrated instruments with field strengths of 53, 99, 215, and 350 gauss were used. In addition, noncalibrated instruments with field strengths of approximately 150 and 350 gauss were used. The energies of lines recorded with these instruments were determined by applying an equation of the type

$$(H\rho)^2 = ax^2 + bx + c, \qquad (2)$$

where x is the position of the line on the plate, and a, b, and c are constants which are evaluated from the positions of lines whose $H\rho$ values had been determined with the calibrated instruments.

Because of the large number of protactinium isotopes present in each sample, several exposures were made in order to follow the decay of the electron lines. In this manner it was possible to distinguish between lines due to 27.4-day Pa^{233}, 17-day Pa^{230}, 1.5-day Pa^{229}, and 22-hour Pa^{228}. Although the half lives of the latter two isotopes are similar, it was possible to prepare Pa^{229} without Pa^{228}, thus simplifying the assignments. The lines due to 1.3-day Pa^{232} could not be distinguished from those of Pa^{229} by following their decay, but since Pa^{232} decays to uranium and Pa^{229} to thorium, the differences in thorium and uranium binding energies may be utilized in making the assignments.

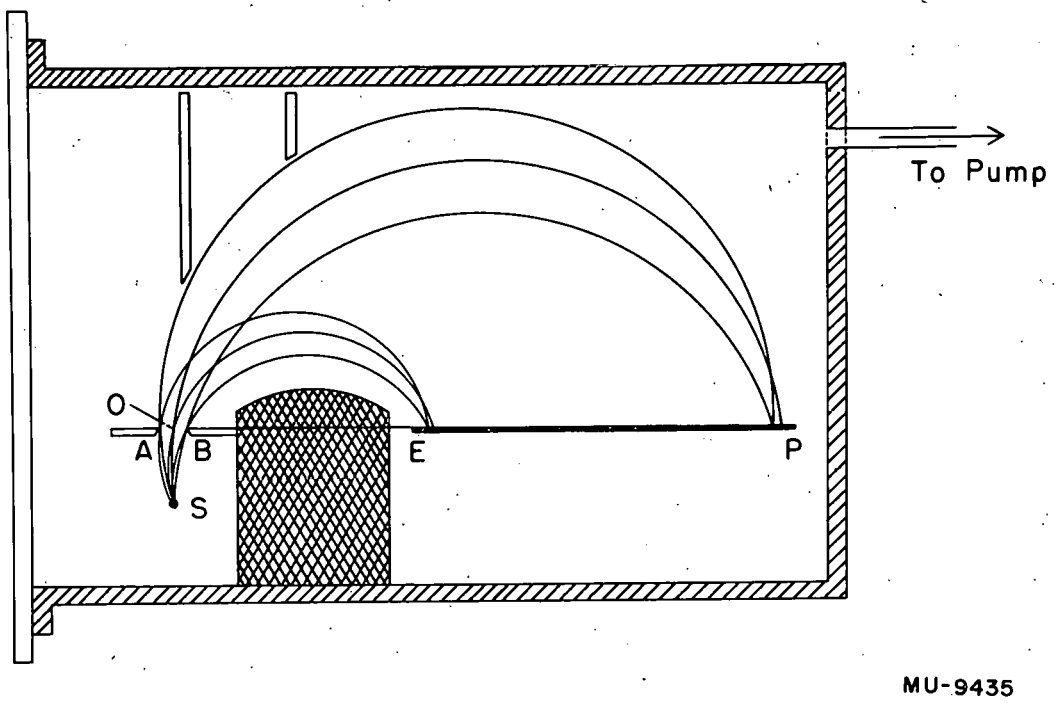

Fig. 5. Schematic diagram of permanent-magnet electron spectrograph.

Because of the extensive and uncertain calibration procedures required for obtaining relative intensities of lines, only rough estimates were recorded in most cases. Densitometer tracings were made on only a very few plates.

C. Gamma-Ray Spectroscopy

During the course of this study various gamma-ray spectrometers were employed, the choice depending upon the type of information desired, the availability of the equipment, and the nature of the sample. By employing coincidence techniques it was possible to obtain spectra of gamma rays in coincidence with photons of any given energy, with all alpha particles, or with alpha particles of a given energy, in addition to straight gamma-ray spectra. A fast-coincidence circuit which permitted delayed coincidences to be run was used to look for metastable states in the alpha decay of Pa^{229}.

Crystals of thallium-activated sodium iodide were used as detectors for gamma rays. In most cases crystals measuring 1-1/2 by 1 inch were employed, although 3-by-3-inch crystals were used in some instances. The light output from the crystal was converted into electronic pulses by a photomultiplier tube. For straight gamma spectra, these pulses were then amplified and fed into a multichannel pulse-height analyzer, where the energy spectrum of the gamma rays was recorded. In the early stages of this work 50-channel pulse-height analyzers were employed, while later, a 100-channel PENCO pulse-height analyzer, permitting use of much more active samples, was used. All gamma-ray intensities have been corrected for escape-peak losses by using Axel's curves,[12] and for counting efficiency by employing the curves of Kalkstein and Hollander.[13]

For gamma-gamma coincidence studies, sodium iodide crystals were used to detect the gate and signal pulses. For alpha-gamma coincidence studies, a zinc sulfide screen sprayed directly onto a photomultiplier tube served as the gate detector.

Since the type of circuit employed varied from one experiment to another, depending upon the nature of the experiment, no circuit diagram

is outlined here. Detailed descriptions of the apparatus used in this type of study have been given by Frank S. Stephens, Jr.[14] and Donald Strominger.[15]

D. Preparation and Purification of Active Materials

1. Bombardment Procedures

The isotopes of protactinium that were studied in this work were all prepared by cyclotron bombardments. The cyclotrons used were the Crocker Laboratory 60-inch cyclotron, which accelerated deuterons to 24 Mev, protons to 12 Mev, and helium ions to 48 Mev; and the 184-inch synchrocyclotron, which accelerates deuterons to 370 Mev, protons to 740 Mev, and helium ions to 885 Mev. In order to take advantage of the high beam intensity and energy selectivity provided by the 60-inch cyclotron, targets of enriched Th^{230} (87% Th^{230} and 13% Th^{232}) were bombarded with deuterons from this machine whenever possible. This enabled isotopes of protactinium of mass number 228 and heavier to be produced by the (d,xn) reactions. In order to produce Pa^{227} it was necessary to employ the higher-energy projectiles of the 184-inch cyclotron.

For bombardments on the 60-inch cyclotron approximately 15 milligrams of the target material in the form of finely powdered thorium chloride was placed in a gold boat, covered with a 0.001-inch platinum foil, and bombarded for 8 to 10 hours with deuterons with a beam intensity of approximately 15 microamperes. Maximum-energy deuterons were used when Pa^{228} was desired, and 17-Mev deuterons when it was not. This latter energy was chosen as the result of calculations showing the threshold for the $Th^{230}(d,4n)Pa^{228}$ reaction to be 17.5 Mev. No radiations characteristic of Pa^{228} – conversion electrons, alpha particles, or gamma rays – were observed following bombardments at 17 Mev.

For producing Pa^{227}, thorium metal (Th^{232}) was bombarded on edge with protons at the minimum accessible radius (45 inches) of the 184-inch cyclotron. This gave approximately 0.5 microampere of 280-Mev protons.

2. Chemical Separations

The problems involved in separating protactinium from other activities

produced in the bombardments outlined above are by no means trivial. Although a vast amount of new information has accumulated during the past few years,[16] the chemistry of protactinium is still not completely understood. Its tendency to undergo hydrolytic polymerization reactions of unknown nature still results in nonreproducibility of chemical behavior, in addition to loss of activity due to adsorption on the walls of containers. The large amount of fission-product activities produced requires that tracer amounts of protactinium be isolated from nearly all other elements in the periodic table and from large amounts of target material. The strict requirement of obtaining a mass-free sample further complicates the problem.

To meet the requirements of obtaining a mass-free sample, radiochemically free from all contaminants, and taking account of the fact that all chemical procedures must be carried out inside a glove box or junior cave within a reasonable length of time, it was decided to avoid the commonly used methods of coprecipitation and concentrate on ion exchange and solvent extraction.

In previous studies of this type,[17,18] the elements which tended to follow protactinium through the chemical procedures used to purify it were zirconium and niobium. Repetition of individual steps in the purification procedures failed to completely remove these activities. In view of this, it was felt necessary to devise means of effecting the separation of protactinium from zirconium and niobium by using ion-exchange methods, if possible.

The method finally selected exploits the differences in behavior when tracer amounts of the three elements are equilibrated with Dowex-1 anion-exchange resin from solutions of hydrochloric acid[19] and from solutions of HCl containing small amounts of HF.[20]

Figure 6 shows the elution curve for a mixture of Th(IV), Zr(IV), Nb(V), and Pa(V) under different eluting conditions. The column used was 3 mm in diameter and was filled to a height of 55 mm with Dowex-1 anion-exchange resin. The column volume, defined as the number of drops required for a band to traverse the length of the resin column, was 5 to 6 drops. In strong HCl solutions, Pa(V) sticks to the resin along with

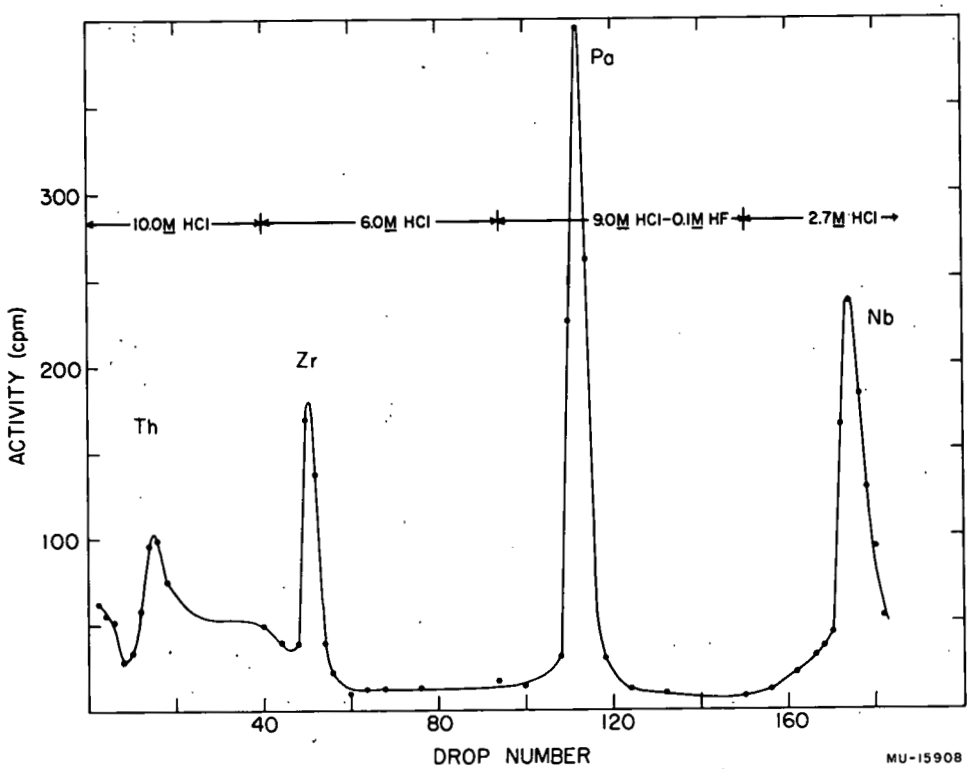

Fig. 6. Separation of Th, Zr, Pa, and Nb on Dowex-1 anion-exchange column.

Zr(IV) and Nb(V), while Th(IV) passes right through along with the other alpha emitters in the periodic table below protactinium. With 6 M HCl as the eluting agent, Zr(IV) is rapidly stripped off in a few column columes with no loss of Pa(V) or Nb(V). The protactinium is then eluted in 9.0 M HCl – 0.1 M HF, completely separating it from Nb(V). The latter may then be eluted in 1 to 4 M HCl. The acid concentrations used here were selected as those giving the best separations in experiments using tracer Pa^{231}, Zr^{95}, and Nb^{95}.

A glance at curves showing the adsorption of the elements from hydrochloric acid onto Dowex-1 anion-exchange resin[19] indicates that the above procedure should separate protactinium from essentially all the other elements. However, to be on the safe side it was felt advisable to perform a solvent-extraction cycle in addition. The solvent selected was diisopropyl ketone (DIPK), and the procedure followed was that outlined by Golden and Maddock[21] with some modifications. The 9.0 M HCl – 0.1 M HF solution containing the protactinium from the anion-exchange column was contacted with an equal volume of DIPK. Under these conditions such species as Fe(III) and Po(IV) extract quantitatively into the DIPK, along with appreciable amounts of Sn(IV), Nb(V), and others. Pa(V) extracts to the extent of less than 0.4%. The solvent phase was then discarded and borax ($Na_2B_4O_7 \cdot 10H_2O$) or anhydrous $AlCl_3$ was added to the aqueous phase. Of these two complexing agents for fluoride ion, it was felt that borax was more suitable. Although $AlCl_3$ seemed to have slightly better complexing characteristics, it appeared to be appreciably soluble in DIPK, and excess quantities in solution gave voluminous precipitates. The aqueous phase was then contacted with an equal volume of fresh DIPK. Under these conditions, Pa(V) extracts quantitatively into the solvent phase, removing it from Th(IV), Ti(IV), V(V), Zr(IV), U(VI), and other species. The protactinium was then re-extracted from the solvent phase into an equal volume of 2.0 M HCl.

To remove all extraneous mass and reduce the volume to a very few drops, the solution containing the protactinium was then made approximately 10 M in HCl and passed through a small anion resin column (3 mm in diameter, 12 mm in height). After being washed with 10 M HCl, the protactinium

was then eluted with 2.7 M HCl. The third through sixth drops, containing more than 90% of the protactinium activity, were then collected on a platinum disc and used for sample preparation.

For recording the alpha-particle spectra of isotopes of protactinium, such extensive purification procedures were not required. In such cases it was necessary only to remove the target material and other alpha emitters. This was done by passing the mixture of activities in approximately 10 M HCl through a small Dowex-1 anion-exchange column (3 by 12 mm). Th(IV) and all alpha emitters below protactinium pass through the column without adsorbing. After the column had been washed with 10 M HCl to remove all traces of these other alpha emitters, protactinium was eluted in four drops of 2.7 M HCl, as outlined above.

Dissolution of target materials also presented some problems. The targets were either thorium metal or $ThCl_4$ powder, some of which was converted to ThO_2 during the bombardments. Although dissolution of both thorium metal and ThO_2 has received special mention in the literature,[22] techniques especially suited to the chemical procedure outlined above were developed in this study. The reagent best suited for dissolution of both the metal and the oxide of thorium was found to be concentrated HCl containing HF as a catalyst. The amount of HF added depended upon the amount of target material to be dissolved and the final volume of solution desired. By slow addition of a dilute HF solution to a known amount of Th(IV) and vice versa, it was found that ThF_4 precipitates when the mole ratio of fluoride to thorium is greater than 2:1. It was also found that the rate of dissolution of thorium metal is a direct function of HF concentration. Hence, it was desired to keep the HF concentration high enough to permit rapid dissolution, but low enough to prevent precipitation of ThF_4, which might also carry down the protactinium activity. Concentrated HCl – 0.01 M HF was used for dissolving the relatively small amounts of powder used in the 60-inch cyclotron bombardments, while the thorium metal bombarded at the 184-inch cyclotron was dissolved in concentrated HCl – 0.2 M HF. The volumes were kept as small as possible while the hydrogen ion concentration, which was depleted by the dissolution process, was kept high enough to permit protactinium to adsorb onto the resin. The fluoride ion was complexed by the addition of borax or $AlCl_3$ before the solution was passed through the column.

Samples for the alpha-particle spectrographs were prepared by evaporating the few drops of solution from the last anion-exchange column onto the tungsten filament, and proceeding as outlined earlier (Section II-A.1). The first few sources were prepared by evaporating the active solution to dryness on the platinum disc and then transferring the activity to the filament by taking it up in concentrated HCl. However, this resulted in considerable broadening of the peaks, presumably due to small amounts of platinum which were scraped from the disc and sublimed with the protactinium.

Samples for the permanent-magnet spectrographs were prepared by evaporating the few drops of solution containing the activity to dryness on the platinum disc, and then taking the activity up in the plating solution and transferring it to the electrolysis cell.

Two different electrolytes were used as plating solutions: 0.81 M NH_4F adjusted to a pH of 6.0, and 0.32 M $(NH_4)_2C_2O_4$ adjusted to a pH of 7. Neither of these solutions gave yields of protactinium exceeding 50%, although both were superior to other electrolytes tried.

Samples for the gamma-ray spectrometers were prepared by simply evaporating the activity onto aluminum, nickel, or platinum discs.

III. EXPERIMENTAL RESULTS

A. Alpha Decay of Pa^{229}

Pa^{229} was first produced by Hyde and Studier, who reported that it decays with a 1.5-day half life and emits alpha particles with an energy of 5.66 Mev.[23] This half life was confirmed by Meinke et al., who determined the alpha branching to be roughly 1% and the energy of the alpha particles to be 5.69 Mev.[24] Later unpublished data of Slater and Seaborg indicate that Pa^{229} decays 99.75% by electron capture and 0.25% by alpha-particle emission.[25] No previous high-resolution spectroscopic measurements of the alpha-particle energies have been reported.

1. Alpha Spectrum

Several alpha spectra of Pa^{229} were obtained in the early phases of this work with the uniform-field spectrograph. However, because of the small alpha branching of this nuclide and the low transmission of the spectrograph, only a few hundred alpha tracks were recorded in exposures of approximately 3 days' duration. The resolution obtained was quite poor owing to the faulty sample-preparation technique mentioned in Section II-D.

The spectra obtained by using the double-focusing magnet were much better. Figure 7 shows a spectrum obtained at high resolution and Fig. 8 shows a spectrum obtained at only moderate resolution while looking for low-intensity alpha groups.

It should be pointed out that the spectrum shown in Fig. 8 contains no contribution from Pa^{228} and its decay products, whereas the spectrum shown in Fig. 7 does. The alpha group designated with a question mark was shown not to be $Ra^{224}_{\alpha_0}$ by both energy and intensity arguments. It is probably not a Pa^{229} alpha group for reasons explained in Section III-A.2, although it cannot be assigned to any other alpha emitter thought to be present. The group designated as α_{252} and α_{264} appears to be composed of two peaks, especially when background is subtracted out, although this is not beyond question. The existence of a group designated α_{356} is very doubtful, although the hump may be real.

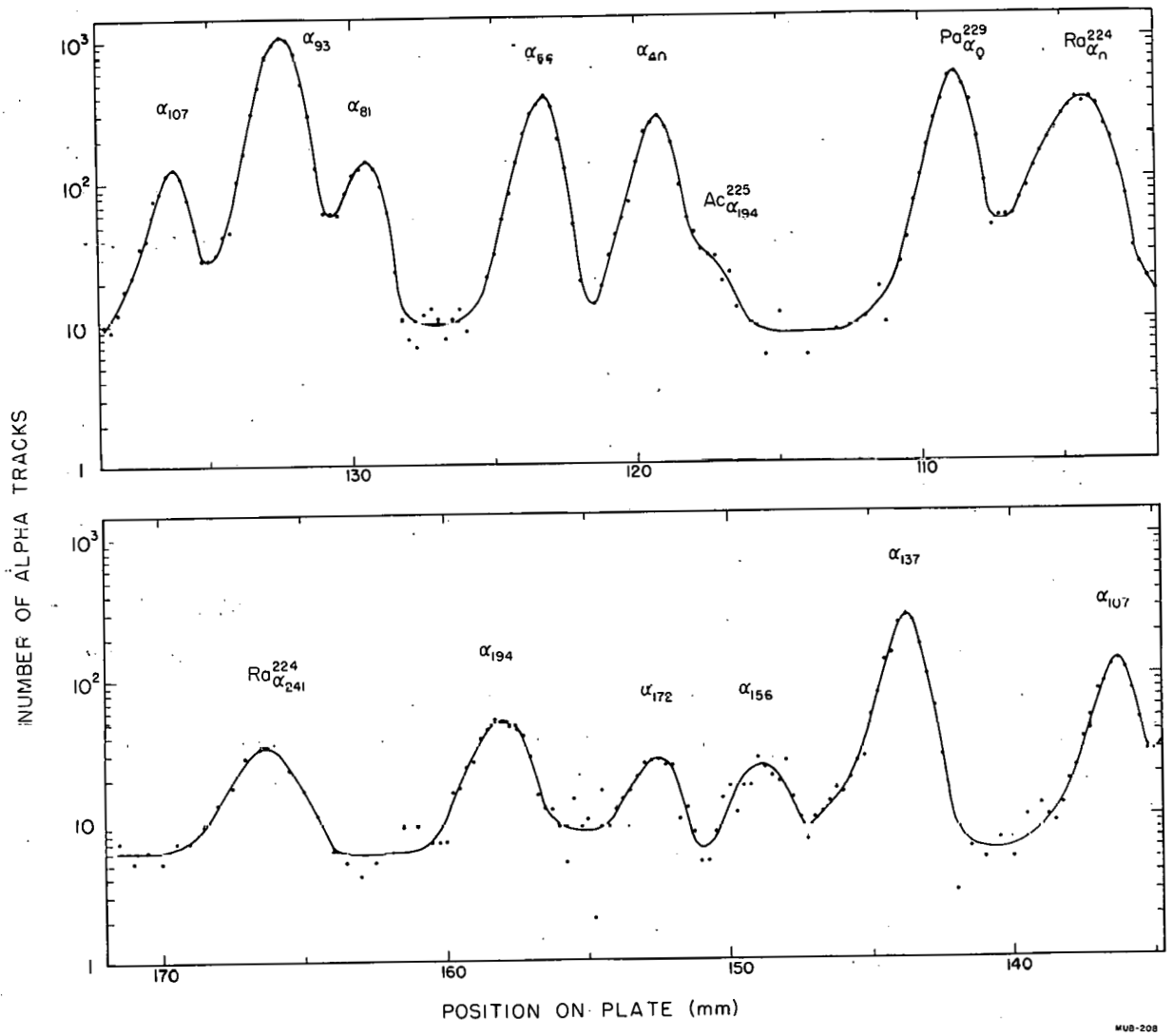

Fig. 7. Alpha-particle spectrum of Pa^{229} at high resolution — double-focusing spectrograph.

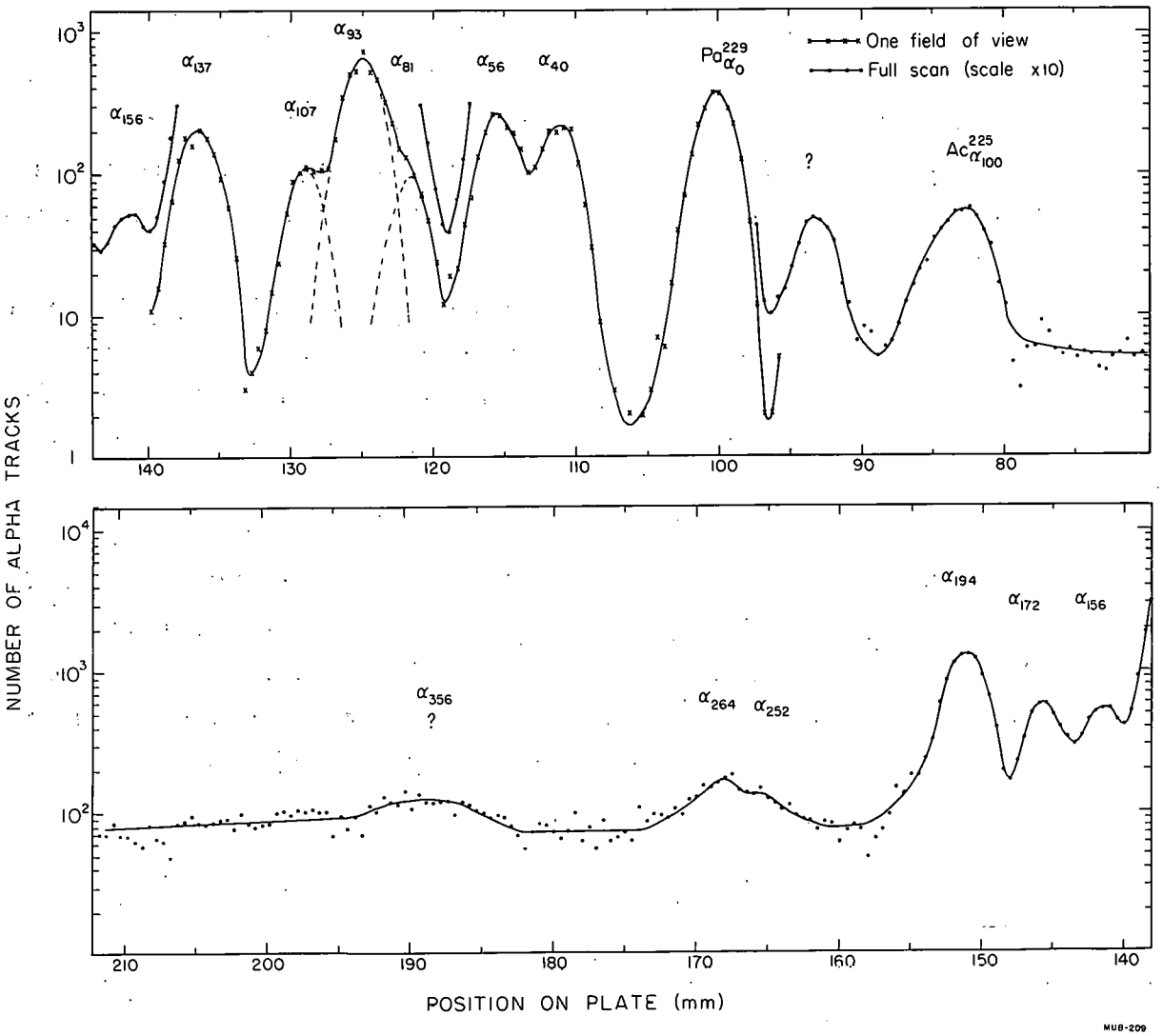

Fig. 8. Alpha-particle spectrum of Pa^{229} — search for low-intensity groups with double-focusing spectrograph.

The absolute energies and energy separations of the alpha groups were obtained by using Eq. (1), with both $Ra^{224}_{\alpha_o}$ and $U^{230}_{\alpha_o}$ employed as standards. The differences in recoil energy associated with the alpha groups were added to the particle energy-separations to give the excited-state-energies. Table II summarizes the energy data from a number of experiments. The adopted values are the average values for all the experiments, and the limits of error shown are the standard deviations. Although certain experiments were felt to be more reliable than others, no substantial difference was obtained by weighting the experiments. The standard deviations decreased by no more than 0.1 kev and the average values changed by no more than 0.2 kev.

Table III summarizes the abundances of the alpha groups observed in a number of experiments. The adopted values are weighted averages and the limits of error represent the standard deviations. In those cases where only a few observations were made, the suspected limits of error are listed.

The energies and abundances of the alpha groups of Pa^{229} are summarized in Table IV, along with the hindrance factors and excited-state energies. The hindrance factor of an alpha group is the factor by which the observed alpha half life differs from that calculated by simple barrier penetration theory. The hindrance factors were calculated by employing the constants of Perlman and Rasmussen.[26]

Table II. Excited-state energies in Pa^{229} alpha decay

Alpha Group	Excited-state energy (kev) Exposure Number 524[a]	567[a]	150-1	150-2	162	173-1	173-2	164	Adopted Values
α_{40}	38.8	41.6	39.4	40.6	41.2	40.4	40.2	40.1	40.3±0.7
α_{56}	56.1	57.2	55.3	56.1	57.1	55.7	56.3	56.4	56.3±0.6
α_{81}	-	-	80.1	80.2	80.8	81.3	80.9	80.5	80.6±0.4
α_{92}	92.2	92.4	91.0	91.3	92.5	91.8	91.9	91.8	91.9±0.5
α_{107}	106.3	106.4	106.3	106.4	108.4	108.3	107.6	108.6	107.3±1.0
α_{137}	135.9	138.8	136.3	136.0	137.8	135.3	136.6	136.7	136.7±1.0
α_{156}	-	-	-	156.2	157.2	154.4	155.9	-	155.9±1.0
α_{172}	-	-	171.7	171.3	173.0	172.1	172.6	171.8	172.1±0.6
α_{194}	-	-	193.7	193.4	194.1	194.0	194.6	194.7	194.1±0.5
α_{252}	-	-	-	-	-	252.5	252.4	-	252.4±0.1
α_{264}	-	-	-	-	-	264.8	262.6	-	263.7±1.1
α_{356}	-	-	-	-	-	356.1	-	-	356.1
E_{α_o} (Mev)	5.665[b]	5.670	5.665	5.665	5.665	5.665[b]	5.665[b]	5.665	5.665

[a] Exposures made on uniform-field spectrograph.

[b] Assumed value – energies relative to $U^{230}_{\alpha_o}$ = 5.884 Mev and $Ra^{224}_{\alpha_o}$ = 5.681 Mev.

Table III. Abundances of Pa^{229} alpha groups

Alpha Group	Abundances (%) Exposure Number 150-1	150-2	162	173-1	173-2	164	Adopted Values
α_0	19.6	18.5	20.7	18.0	-	-	19.1±0.8
	19.6	19.5	18.8	18.1	18.5	19.7	
α_{40}	8.9	9.5	9.6	11.3	-	-	9.8±0.9
	8.1	9.6	10.6	10.2	10.2	10.5	
α_{56}	12.1	12.9	14.2	13.3	-	-	13.4±0.8
	12.8	13.6	13.9	12.7	15.5	13.9	
α_{81}	3.8	4.4	5.5	4.1	-	-	4.7±0.5
	4.2	4.6	5.3	5.4	4.7	5.3	
α_{92}	39.4	38.5	34.6	35.4	-	-	36.8±1.7
	39.0	36.9	36.1	35.4	37.8	34.9	
α_{107}	3.9	3.9	3.7	3.4	-	-	3.9±0.3
	3.9	4.1	3.7	4.9	4.2	3.9	
α_{137}	8.3	8.4	8.7	10.7	-	-	8.9±0.8
	8.9	8.7	9.0	9.8	5.8	7.9	
α_{156}	0.60	0.81	0.46	0.69	-	-	0.60±0.11
	0.53	0.58	0.41	0.69	0.61	-	
α_{172}	1.2	0.88	0.63	0.76	-	-	0.74±0.10
	0.86	0.66	0.57	0.75	0.72	1.1	
α_{194}	1.86	1.90	1.56	2.06	-	-	1.77±0.21
	1.79	1.43	1.30	1.80	1.80	2.0	
α_{252}	-	-	-	0.08	-	-	0.07±0.02
	-	-	-	0.08	0.05	-	
α_{264}	-	-	-	0.20	-	-	0.15±0.04
	-	-	-	0.14	0.11	-	
α_{356}	-	-	-	-	-	-	0.05±0.04
	-	-	-	-	0.05	-	

Upper figures in each group are integrated intensities.
Lower figures are based on peak heights.

Table IV. Alpha groups of Pa^{229}

Alpha-particle energy (Mev)	Excited-state energy (kev)	Abundance (%)	Hindrance factor
5.665	0.0	19.1	23.
5.625	40.5	9.8	28.
5.610	56.3	13.4	170
5.586	80.6	4.7	36.
5.575	91.9	36.8	4.0
5.560	107.3	3.9	31.
5.531	136.7	8.9	9.4
5.512	155.9	0.60	110.
5.496	172.1	0.74	73.
5.474	194.1	1.77	23.
5.417	252.4	0.07	280.
5.408	263.7	0.15	115.
5.315	356.0	0.05	100.

2. Alpha - Gamma Coincidence Spectrum

Because of the small alpha branching of Pa^{229}, coincidence techniques must be applied in order to observe the de-excitation of levels populated in its alpha decay. In this study, the gamma rays in coincidence with total alpha particles were examined with scintillation spectrometers. Since no energy discrimination was made on the alpha particles giving rise to the gate pulses, it was essential that Pa^{229} be the only alpha activity present. This was assured by bombarding below the $Th^{230}(d,4n)Pa^{228}$ threshold and taking the spectrum immediately after the chemical separation. This reduced the contribution from the U^{230} decay series, which grows in quite rapidly from the beta decay of Pa^{230}.

Figure 9 shows a typical alpha-gamma coincidence spectrum. Several of these spectra were obtained by using samples from different bombardments. In all cases the spectra were identical. The abundances of the gamma rays are summarized in Table V.

Table V. Abundances of gamma rays in Pa^{229} alpha decay

E_γ	Abundance (photons per alpha particle)			
	Exp. 1[a]	Exp. 2[b]	Exp. 3[c]	Adopted
40	0.095	0.103	0.103	0.10
69	0.048	0.050	0.071	0.05
81	0.027	0.021	-	0.02
92	0.145	0.163	0.164	0.16
107	0.047	0.048	0.057	0.05
120	0.020	0.017	0.019	0.02

[a] Spectrum recorded on 100-channel PENCO pulse-height analyzer using slow-coincidence apparatus.

[b] Spectrum recorded on 50-channel pulse-height analyzer using fast-coincidence apparatus. Since number of gates could not be recorded, intensities were normalized to 40-kev gamma ray of experiment No. 3.

[c] Spectrum recorded on 50-channel pulse-height analyzer using slow coincidence apparatus.

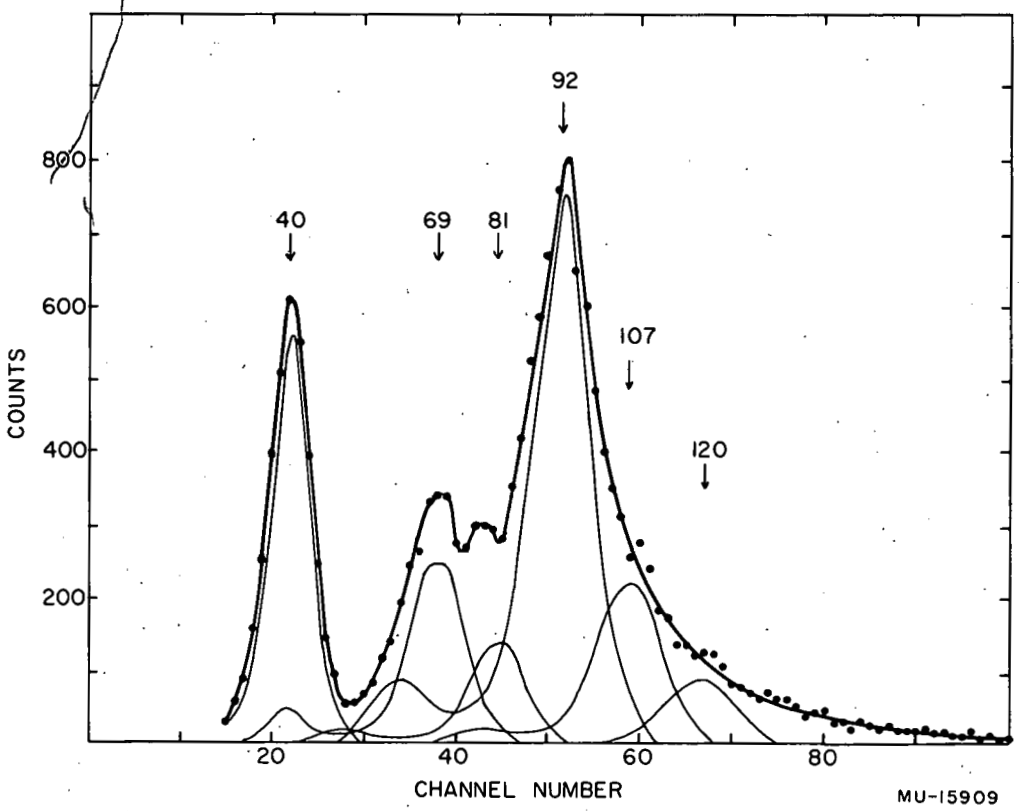

Fig. 9. Alpha particle — gamma ray coincidence spectrum of Pa^{229}.

Although the comparatively weak gamma rays of 69, 81, 107, and 120 kev appear in each spectrum, there is some question as to whether or not they actually belong in the alpha decay of Pa^{229}. The higher-energy gamma rays appear only as a high-energy shoulder on the very prominent 92-kev peak. This shoulder becomes more pronounced with time as the 112-kev gamma ray of Th^{226} grows in. The 69-kev gamma ray appears at the same position as platinum K x-rays and, although aluminum backing plates were used, the activity was transferred from platinum discs. The 81-kev gamma ray appears as a low-energy shoulder on the 92-kev peak, and its intensity is very sensitive to the resolution of the large peak.

Since actinium and thorium K x-rays would appear at 90 to 93 kev, higher-energy gamma rays were looked for to see if internal conversion of higher-energy gamma rays were contributing to the peak at 92 kev. None was observed in sufficient intensity to contribute significantly to the 92-kev peak.

From the abundances of the gamma rays and populations to the various levels in Ac^{225} it is easily shown that both the 40-kev and 92-kev transitions are E1 in nature. Since no more than 81% of the alpha decay may proceed through the level at 40 kev, the total conversion coefficient of the 40-kev transition must be less than 7.1. The theoretical total conversion coefficients for 40-kev E1, M1, and E2 transitions are 1.4, 91, and 1030 respectively,[27] which rules out all but the E1 assignment.

Since no more than 53% of the alpha decay may proceed through the level at 92 kev, the total conversion coefficient of the 92-kev transition must be less than 2.3. The theoretical total conversion coefficients for 92-kev E1, M1, and E2 transitions are 0.16, 9, and 15 respectively, again making the E1 choice unique.

Similar arguments may be advanced to show that the 69-, 81-, and 107-kev transitions must also be E1 in nature if their abundances are those shown in Table V.

Attempts to obtain the spectrum of gamma rays in coincidence with alpha particles of a given energy failed to give good results, although they did provide some useful information. By gating on the most intense alpha group, designated α_{92}, it was found that the coincidence rate was

0.25 to 0.4 photon per alpha particle. The photons all appeared to be in the 92-kev energy region. The same photon energy and same coincidence rate were obtained by gating on the alpha group designated α_{137}. These results were based on only a comparatively few events (10 to 200 coincidences) and cannot be considered conclusive nor unambiguous.

Because of the presence of these E1 transitions in the alpha decay of Pa^{229}, and the existence of several E1 transitions with measureable lifetimes in this region (for example, the 27-kev transition in the alpha decay of Pa^{231}), it seemed advisable to look for metastable states. A fast coincidence circuit permitting delayed coincidences to be run was used to measure the half lives of the states de-excited by the E1 transitions following Pa^{229} alpha decay. The transitions were all found to be prompt, and the following upper limits were set for the half lives of the states de-excited by the 40-, 69-, and 92-kev transitions respectively: 1.5×10^{-9} sec, 2.0×10^{-9} sec, and 2.7×10^{-9} sec. It seems reasonable to assume that the prompt 40-kev E1 transition is the same as Stephens observed in Ac^{225} following Ra^{225} beta decay.[28] He set a limit of 2×10^{-9} sec for its half life and determined its total conversion coefficient to be approximately 1.1.[14]

Since he saw only the 40-kev gamma ray and just enough L x-rays to account for its internal conversion, and failed to observe any radiations at all in coincidence with the 40-kev photons, it is safe to assume that the transition is to the ground state of Ac^{225}. It is for this reason that the unassigned alpha group shown in Fig. 8 is not assigned to Pa^{229}. If this group did belong to Pa^{229}, the ground state would be 25.9 kev lower in energy and a level 40 kev above this would be populated in Ra^{225} beta decay. Of course, this is still possible if the 40-kev E1 transition observed in this study is not the same as that observed by Stephens. For the present, it is assumed that they are the same.

3. Decay Scheme

The alpha decay scheme of Pa^{229} is shown in Fig. 10. Only those transitions which are felt to be certain are shown, although others, such as those included in Table V, may have been observed, and still others may be inferred from intensity considerations.

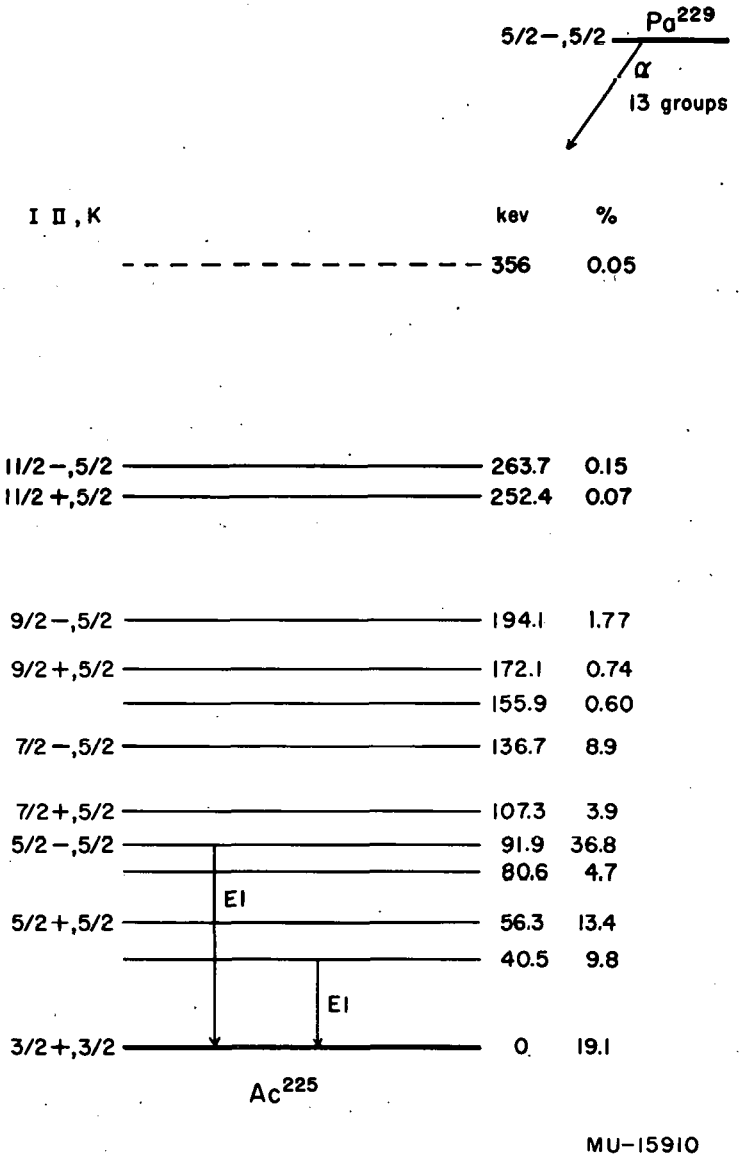

Fig. 10. Alpha decay scheme of Pa^{229}.

If the theoretical total conversion coefficient of 1.4 is assumed for the 40-kev E1 transition, this requires that 24% of the decay proceed via this transition. Since the alpha population to the level is only 9.8%, this requires that an additional 14% of the alpha decay cascade through the level at 40 kev. The population to the next higher level could easily account for this, although alternative cascades could also be proposed.

As was pointed out in Section III-A.2, the coincidence spectrum displayed by gating on both α_{92} and α_{137} showed only 92-kev photons in an abundance of 0.25 to 0.4 photon per alpha particle. This indicates that the total conversion coefficient of the transition is 1.5 to 3.0 (E1 with perhaps a very small admixture of M2). Since the abundance of the photons is 16%, this would account for 40 to 64% of the total alpha decay. As the population to the level is 36.8%, and the total population to it and all higher levels is 53%, these wide limits allow no conclusions to be made concerning possible cascades.

4. Interpretation of Levels

Since there is reason to believe that Ac^{225} might still exhibit a more or less stable spheroidal deformation, it might also be expected to exhibit some of the characteristics predicted by the Bohr-Mottelson collective model for nuclei in this region. The most striking feature predicted by this model is the occurrence of rotational bands. The energy-level spacings of such a rotational band are given by

$$E_I = \frac{\hbar^2}{2\Im} [\, I\,(I+1) - I_o\,(I_o+1)\,] \,, \qquad (3)$$

where E_I is the energy of the level with spin I above the base member of the band, $\Im$ is the moment of inertia, and I_o is the spin of the base member.* For odd-mass nuclides, allowable spins are I_o, $I_o + 1$, $I_o + 2$, etc. A characteristic of members of a rotational band is the fact that the component of total

*For the case of $I_o = 1/2$, an additional term $\Delta E_I = \frac{\hbar^2}{2\Im} a\,(-)^{I+1/2}(I + 1/2)$ must be added to Eq (3), where a, the decoupling parameter, is a constant for each band.

angular momentum along the nuclear symmetry axis (K-quantum number) is the same for each member and is equal to the spin of the lowest member, I_o.

It has become increasingly evident during the past few years that almost every odd-mass alpha emitter in the Bohr-Mottelson region exhibits essentially unhindered alpha decay to a rotational band of its daughter nucleus. It is supposed that such a transition leaves the intrinsic wave function of the odd nucleon unchanged and is thus exactly analogous to the alpha transitions to the ground-state rotational band in even-even nuclei. The term "favored" alpha decay is usually applied to these transitions. Bohr, Froman, and Mottelson[29] have recently developed a relationship between the population of alpha groups to members of a favored rotational band and to the ground-state rotational band in even-even nuclei. Very good agreement is shown between these calculated intensities and those found experimentally for a number of odd-mass alpha emitters.[26,29]

One of the more prominent features of Pa^{229} alpha decay is the relatively large population to the level at 92 kev. If "favored" alpha decay is exhibited, it is to this state. Inspection of the decay scheme also reveals the presence of another state just 44.8 kev higher in energy with a relatively low hindrance factor. These two features alone suggest a close similarity to several other cases of favored alpha decay found in this region with similar energy-level spacings and relative hindrance factors. Five such cases have been noted, all with energy separations of 43 to 46 kev and $K = 5/2$.[26]

With the assumption $K = I = 5/2$ for the level at 93 kev and $I = 7/2$ for the level at 137 kev, the rotational constant $\hbar^2/2\mathfrak{I}$ is found to be 6.40 kev for the rotational band. Use of this value in Eq. (3) enables the energies of the next higher members to be calculated. Table VI compares the calculated energies with those found experimentally. The agreement is even better than might be expected, and implies that there are no near-lying states of the same parity with $K = 5/2 \pm 1$.

Although the hindrance factor for the alpha group populating the level at 92 kev is not unity, as it should be for favored alpha decay, this does not rule out such a possibility. The hindrance factors were calculated by using 0.25% as the alpha branching of Pa^{229}. If the value of

Table VI. Energies of Ac^{225} K = 5/2 rotational band

Spin of state	Excited-state energy (kev)	
	Theoretical	Experimental
5/2	(91.9)[a]	91.9
7/2	(136.7)[a]	136.7
9/2	194.3	194.1
11/2	264.7	263.7

[a]Experimental values used to evaluate rotational constant $\hbar^2/2\Im$ = 6.40 kev.

Table VII. Favored alpha intensities to Ac^{225} K = 5/2 band

Excited-state energy (kev)	Spin of state	Relative intensities	
		Theoretical	Experimental
91.9	5/2	100	100
136.7	7/2	21	24
194.1	9/2	4.1	4.8
263.7	11/2	0.2	0.4

C_o = 1.00 C_2 = 1.00 C_4 = 0.083

approximately 1% reported by Meinke[24] were used, the hindrance factors would all be decreased by a factor of 4. In view of the uncertainty of this alpha branching ratio, it is not unreasonable to assume that the alpha decay to the level at 92 kev in Ac^{225} is of the favored type.

Making this assumption, one may then proceed to calculate the relative alpha populations to the members of the rotational band. The relative transition probabilities according to Bohr, Froman, and Mottelson[29] are given by

$$P = P_o(Z,E) \sum_L C_L \, (I_i LKO | I_i L I_f K)^2, \qquad (4)$$

where C_L is the reciprocal of the hindrance factor for the alpha group of angular momentum L in neighboring even-even nuclei, and the squared term is the Clebsch-Gordan coefficient describing the distribution of the various alpha waves among the members of the rotational band. $P_o(Z,E)$ is a barrier-penetration factor containing the energy and atomic-number dependence for each level and is evaluated from the one-body theory of alpha decay by using the same constants employed in hindrance-factor calculations.[26]

Table VII compares the calculated and experimental relative alpha populations to members of the K = 5/2 rotational band. The C_L's were evaluated from the neighboring even-even nuclides U^{230} and Th^{228}. The agreement is again quite satisfactory, and equally as good as that found for the other cases analyzed to date.[26]

Inspection of the decay scheme reveals another set of levels with energy spacings similar to, although somewhat larger than, those of the rotational band just discussed. The hindrance factors of this second set of levels also increase in about the same proportion as those of the first band, although they are all consistently higher. With the assumption $I_o = 5/2$ for the lowest member of the band and use of the energy separation of the first two members to evaluate the rotational constant, the energies of the next higher members are calculated by using Eq. (3). Table VIII compares the calculated energies with those found experimentally. Again the agreement is good, although the existence of a level at 252 kev is subject to question, as was indicated in Section III-A.1.

Table VIII. Energies of second K = 5/2 rotational band in Ac^{225}

Spin of state	Excited-state energy (kev)	
	Theoretical	Experimental
5/2	(56.3)[a]	56.3
7/2	(107.3)[a]	107.3
9/2	172.9	172.1
11/2	253.1	252.4

[a]Experimental values used to evaluate rotational constant $\hbar^2/2\Im$ = 7.29 kev.

Although this is not a case of favored alpha decay, the Bohr-Froman-Mottelson treatment may be applied to calculate the relative alpha populations to members of this band. In this case L = 1 and L = 3 alpha waves are employed, and the C_L's are evaluated from the hindrance factors of the L = 1 and L = 3 waves in U^{230} and Th^{228} alpha decay. The results of this calculation are shown in Table IX. Although the agreement is not perfect, it is surprisingly good.

Table IX

Alpha intensities to second K = 5/2 band in Ac^{225} (unfavored)

Excited-state energy (kev)	Spin of state	Relative intensities	
		Theoretical	Experimental
56.3	5/2	100	100
107.3	7/2	27	29
172.1	9/2	3.0	5.5
252.4	11/2	0.3	0.5

$C_1 = 0.077$ $C_3 = 0.019$

The results of the calculations shown above indicate the presence of two K = 5/2 rotational bands of opposite parity, since one is populated by alpha waves of even angular momentum, the other by alpha waves of odd angular momentum. The assumption of favored alpha decay requires that the intrinsic wave function of the state at 92 kev be exactly the same as

the ground state of Pa^{229}. In order to identify the intrinsic states involved, the Nilsson diagram for protons, shown in Fig. 11, is employed. This diagram shows the results of Nilsson's calculations[30] considering the effect of a prolate spheroidal deformation of the nucleus on the shell-model energy levels. The energy of the levels is plotted against the amount of spheroidal deformation given in terms of a parameter δ, which is defined as (R major - R minor)/R average. For the case of no deformation, $\delta = 0$, and the usual shell-model levels are observed. As δ increases, however, these shell-model levels split into a number of components, each of which may accomodate two nucleons. These components are designated by the quantum numbers Ω, the symmetry-axis component of total nuclear angular momentum; π, the parity; N, the principal oscillator quantum number; n_Z, the symmetry-axis oscillator quantum number; and Λ, the symmetry-axis component of orbital angular momentum.

The small arrow in the diagram of Fig. 11 indicates the position of the level believed to represent the ground state of Np^{237} (93 protons). Since protactinium has two fewer protons, the ground states of its isotopes should correspond to the next lower level, designated 1/2- (530). It is presently believed that the ground states of both Pa^{231} and Pa^{233} are the 3/2 rotational band members of this (530) intrinsic state.[31] At smaller deformation, which would be expected for Pa^{229}, this level crosses the 5/2- (523) level, which would correspond nicely to the ground state of Pa^{229}. The next lower state, which would be expected to be the ground state of the nuclide with two fewer protons, is designated 3/2+ (651), and is thought to be the ground state of Ac^{227}.[31] The same assignment for the ground state of Ac^{225} would fit in nicely with the decay scheme shown in Fig. 11, since there is an El transition from the 92-kev level to ground.

The level at 40 kev might easily be a rotational band member of the 1/2- (530) state which lies just above the 3/2+ (651) state and would also de-excite by means of an El transition.

The only 5/2+ intrinsic state in this vicinity is the 5/2+ (642) state, which lies considerably above the 5/2- (523) state for this amount of distortion. An alternative explanation for this 5/2+ band is to

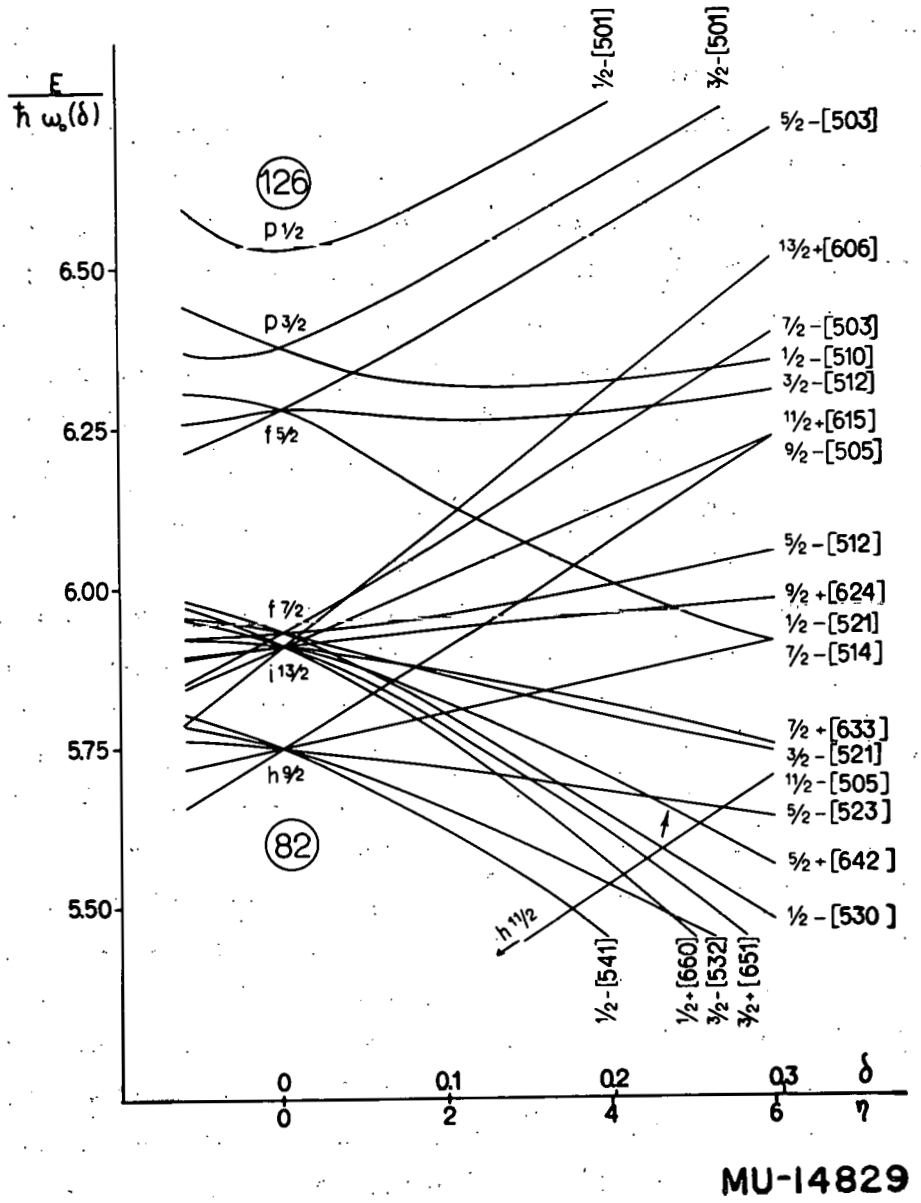

Fig. 11. Nilsson diagram for 82 to 126 nucleons.

associate it with the 5/2- band and assume that both represent the same intrinsic state. In other words, the 5/2+ band is analogous to the odd-parity states in even-even alpha decay. Froman[32] has indicated that favored alpha groups of odd parity should be expected in odd-mass nuclei in this region, although none has been found. He further indicates that the two bands populated by the alpha groups of even and odd parity should have opposite parity and similar energy-level spacings, and be displaced with respect to each other by roughly the same amount as the even and odd parity bands in neighboring even-even nuclei. All these characteristics are found in the alpha decay of Pa^{229}, except the energy displacement of the two bands. However, since no satisfactory explanation has been offered for the relative displacements of the two bands in even-even nuclei, it might be possible for the band populated by the odd alpha waves to lie lower in energy. This might possibly result from a stabilized asymmetry in the shape of the nuclear surface of the pear- or egg-shaped variety mentioned by Bohr et al.[29]

The fact that the hindrance factors for these alpha groups of odd parity are so small is further evidence that the decay is taking place between the same intrinsic state in parent and daughter. In the alpha decay of Am^{241}, unfavored decay from the 5/2- (523) state to the 5/2+ (642) state in Np^{237} is hindered by a factor of about 700. In Pa^{229}, the odd-parity alpha groups are hindered to a lesser extent than in the neighboring even-even nuclei U^{230} and Th^{228}. By making use of the Bohr-Froman-Mottelson Eq. (4), and using the hindrance factors for both even- and odd-L alpha waves from U^{230} and Th^{228}, one can calculate the relative alpha populations to all eight levels and compare them with the experimental values. The results are shown in Table X. It is seen that the experimental values are higher by a factor of about five than those predicted for the 5/2+ band. If hindrance factors of 2.0 and 8.0 for the L = 1 and L = 3 waves are used, the agreement is much better (Table X). Justification for the use of lower hindrance factors is found in the alpha decay of Ra^{224}, Th^{226}, and Ra^{222}, which have L = 1 hindrance factors of 2.3, 2.4, and 0.97, respectively.[26] It is obvious that adjustment of the C_L's and use of C_5 would give even better agreement.

Table X. Favored alpha intensities to K = 5/2 bands in Ac^{225}

Spin and parity of state	Relative intensities		
	Experimental	Theoretical[a]	Theoretical[b]
5/2-	100	100	100
7/2-	24	21	21
9/2-	4.8	4.1	4.1
11/2-	0.4	0.2	0.2
5/2+	36	6.5	42
7/2+	11	1.8	12
9/2+	2.0	0.2	1.3
11/2+	0.2	0.02	0.2

[a] $C_o = 1.00$, $C_2 = 1.00$, $C_4 = 0.083$; $C_1 = 0.077$, $C_3 = 0.019$.

[b] $C_o = 1.00$, $C_2 = 1.00$, $C_4 = 0.083$; $C_1 = 0.50$, $C_3 = 0.13$.

If the above interpretation were valid, several E1 transitions between states of different parity might be expected. However, most of them could not be observed because of their weak intensities and the presence of the very prominent 40- and 92-kev E1 transitions. The weak 81-kev E1 gamma ray shown in Fig. 9 might correspond to the transition between the 7/2- and 5/2+ states at 136.7 and 56.3 kev. Making use of selection rules for internal transitions in the Nilsson model, one might expect the E1 transition between the 5/2- (523) level at 92 kev and the 3/2+ (651) ground state to be greatly retarded, since $\Delta n_z = 3$. Strominger and Rasmussen have used Nilsson's wave functions to calculate the lifetimes of the possible E1 transitions between different intrinsic nuclear states in this region,[33] and indicate that this particular transition is hindered by a factor of 6×10^4 over the single-particle estimate of Moszkowski. This corresponds to a partial photon half life of 9.5×10^{-9} sec. Assuming $\alpha_{total} = 2.0$, this gives 3.2×10^{-9} sec as the half life of the state. However, their transition probabilities are very sensitive to small details of the wave functions, and any shortcomings of the model will be strongly reflected in their results. Since their calculations for the 60-kev transition in Np^{237} was off by a factor of 25, the above calculation could easily be off by a factor of 2, giving agreement with the experimental half life of $\leq 1.5 \times 10^{-9}$ sec. It is entirely possible that this transition could compete favorably with the alternative 35.6-kev E1 transition to the state at 56.3 kev, which would have the same individual particle configuration.

No satisfactory interpretation can be offered as yet concerning the identity of the remaining levels populated in Pa^{229} alpha decay.

B. Electron-Capture Decay of Pa^{229}

The only previously reported study of the electron-capture decay of Pa^{229} was by Ong Ping Hok,[18] who reported two conversion lines of a 41.7-kev transition.

1. Electron Spectrum

The conversion electrons accompanying the electron-capture decay of Pa^{229} were studied with permanent-magnet spectrographs, and the

assignments were made by methods outlined in Section II-B. The results of these studies are shown in Table XI.

Table XI. Conversion lines of Pa^{229}

Electron energy (kev)	Relative intensity[a]		Shell	Transition energy (kev)
21.92	m	15	L_I	42.37
22.70	ms	25	L_{II}	42.37
26.09	s	30	L_{III}	42.37
37.19	wm	3	M_I	42.35
37.56	m	10	M_{II}	42.37
38.29	m	9	M_{III}	42.32
41.10	wm	13	N_{II}	42.25
41.34	wm		N_{III}	42.28
			Adopted value- - - - - -	-42.37

[a] m = moderate, s = strong, w = weak, ms = moderate to strong, wm = weak to moderate.

Figures represent relative intensities obtained from densitomer tracings.

The relative subshell ratios indicate that the transition is 95% E2 − 5% M1. No other transitions were observed that could be ascribed to the electron-capture decay of Pa^{229}. The same is true of the gamma-ray spectra that were taken. No gamma rays were observed that could be ascribed to the electron-capture decay of Pa^{229}.

2. Decay Scheme and Interpretation of Levels

The electron-capture decay scheme of Pa^{229} is shown in Fig. 12. No estimate can be made of the branching ratio to the two states that are populated in the decay.

The levels in Th^{229} have previously been identified as members of a K = 5/2 rotational band populated by favored alpha decay from U^{233}.[34] Newton has assigned the Nilsson level 5/2+ (633) to the ground states of both U^{233} and Th^{229}.[35]

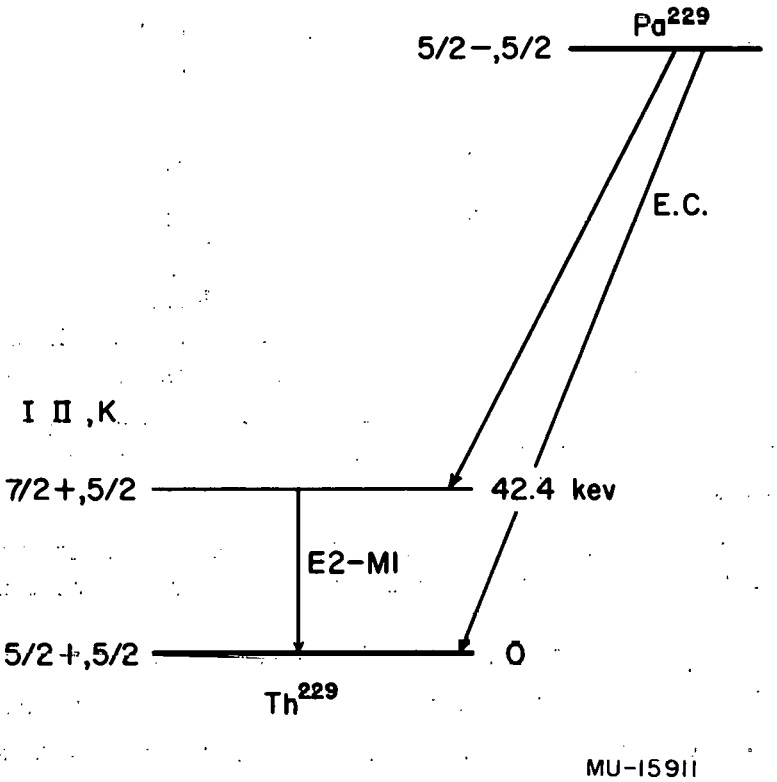

Fig. 12. Electron-capture decay scheme of Pa^{229}.

The fact that the electron-capture decay of Pa^{229} populates the I = 7/2 member of the rotational band is further evidence that the spin of Pa^{229} is 5/2, and not 3/2 as it is in Pa^{231} and Pa^{233}. If this level receives from 0.4% to 40% of the electron-capture decay (which it probably does), the log (ft) for the transition would lie in the range 6 to 8. This corresponds to a first-forbidden, unhindered transition with $\Delta I = 0$ or 1 and a change in parity. The Nilsson level assignment of 5/2- (523) for the ground state of Pa^{229} is thus consistent with the decay scheme.

It should be stressed that other levels could be weakly populated in this decay and escape detection. No limits were set for the population of the other states, although none was observed.

C. Alpha Decay of Pa^{228}

The only previous study of the alpha decay of Pa^{228} was made by Meinke, who reported that it decays 98% by electron capture and 2% by alpha-particle emission, with a total half life of 22 hours.[24] He reported ion-chamber measurements of two alpha groups of 6.09 Mev (75%) and 5.85 Mev (25%).

1. Alpha Spectrum

The alpha-particle spectrum of Pa^{228} was recorded with the aid of the double-focusing spectrograph. In view of the great complexity of the spectrum and comparatively large energy region which it encompassed, it was necessary to make several exposures in order to determine the optimum field settings, slit widths, baffle openings, etc. For best results, 0.010-inch defining slits were used with baffle openings of 1.5 cm. As a result of focusing the peaks away from the ends of the plate, the distortion in peak shape was relatively small, although peaks at either end were slightly broadened. Samples with approximately 3 to 4 x 10^6 total alpha disintegrations per minute were used. Since there were other alpha groups in this region, it was also necessary to follow the decay of the peaks very closely in order to make the correct assignments. A typical

spectrum is shown in Fig. 13. Figure 14 is a spectrum recorded over the same energy region after the Pa^{228} had decayed out.

As might be expected in view of the odd-odd nature of Pa^{228} and its position in the periodic table, the spectrum is very complex. Twenty-three alpha groups are observed, some of which are still complex. Resolution of these peaks gives a total of 27 alpha groups which is the largest number recorded for any nuclide to date, Th^{227} following with 15.[8]

Table XII summarizes the energy data for a number of exposures and Table XIII lists the relative abundances of the alpha groups. As can be seen from the standard deviations, the excited-state energies are good to ± 0.5 kev. The abundances are good to about 5% -- slightly better for the more abundant groups and worse for low-intensity groups. Table XIV summarizes the Pa^{228} alpha-decay data.

The alpha-particle energies were all determined relative to $U^{230}_{\alpha_o}$ = 5.884 Mev. With this standard it was found that the three Ac^{225} alpha groups were consistently 5 kev higher in energy than reported by Hummel relative to Po^{218}.[36] This was also true of the Fr^{221} alpha groups. The energies of the alpha groups of Bi^{212} and Ra^{224} agreed with the presently accepted values.[26]

2. Alpha-Gamma Coincidence Spectrum

The spectrum of gamma rays in coincidence with total alpha particles from a source containing Pa^{228} and Pa^{229} is shown in Fig. 15. As would be expected, the spectrum is very complex. The curve has been resolved into several components, but the resolution is highly uncertain and both the energies and intensities are subject to question. Table XV lists the energies and relative intensities of these gamma rays. Absolute intensities are not given, since the relative amounts of Pa^{228} and Pa^{229} were not determined.

3. Decay Scheme and Interpretation of Levels

The alpha decay scheme of Pa^{228} is shown in Fig. 16. No internal transitions are included because of lack of suffucient information to place them. In order to determine how the levels are de-excited it will

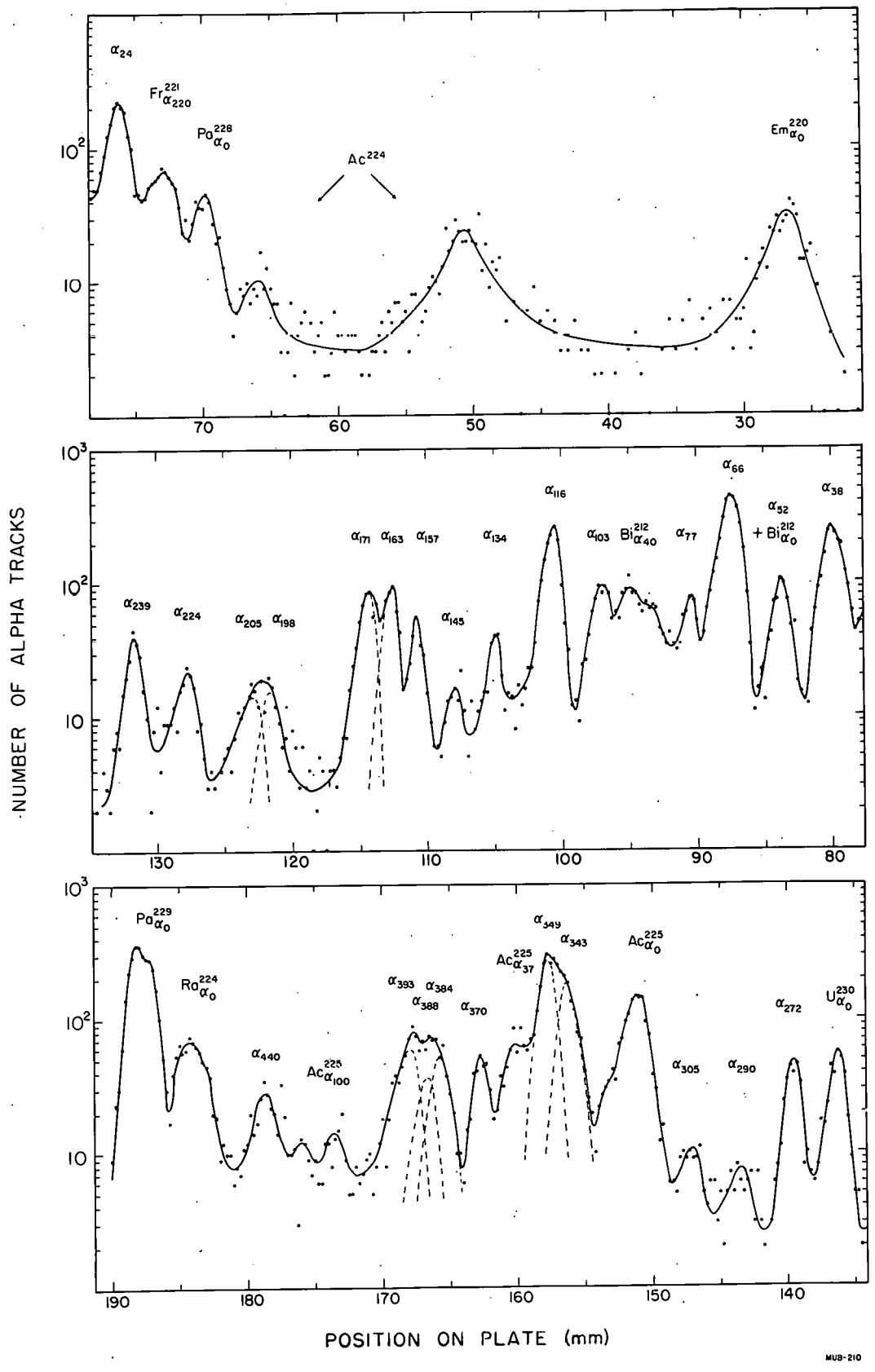

Fig. 13. Alpha-particle spectrum of Pa^{228}—double-focusing spectrograph.

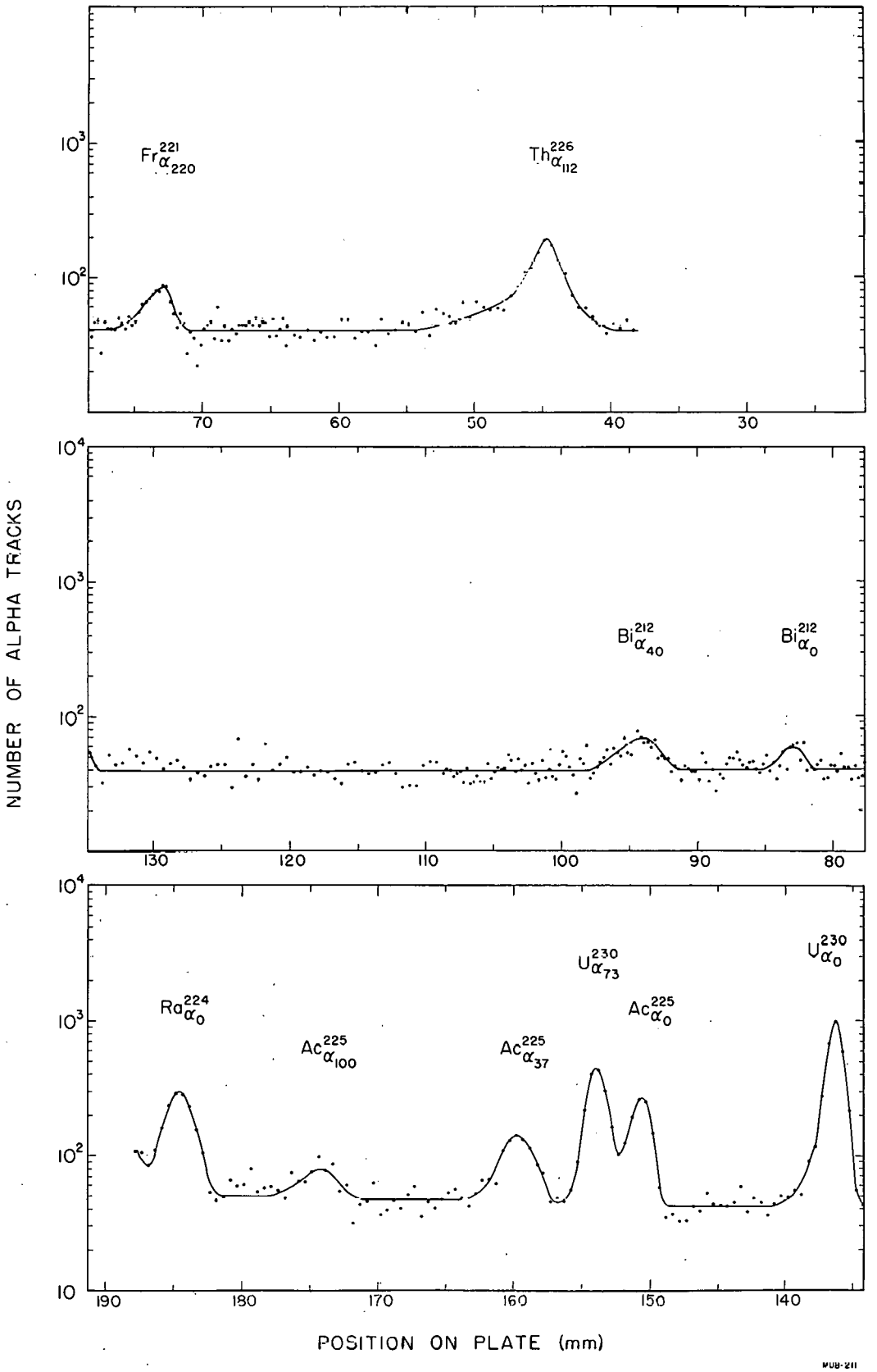

Fig. 14. Alpha-particle spectrum recorded after decay of Pa^{228} — double-focusing spectrograph.

Table XII. Excited-state energies in Ac^{224}

Alpha group	Excited-state energies (kev) Exposure number 148	149	160	161	Average (Adopted)
α_{24}	24.3	23.8	23.8	24.0	24.0±0.2
α_{38}	38.6	37.7	38.1	37.9	38.1±0.3
α_{52}	52.6	51.9	51.9	52.0	52.1±0.3
α_{66}	66.9	66.5	65.8	65.9	66.3±0.4
α_{77}	77.6		77.5	76.4	77.2±0.5
α_{103}	103.3	103.2	102.3	102.4	102.8±0.5
α_{116}	117.0	115.8	116.0	116.6	116.4±0.5
α_{134}	134.0		133.0	133.7	133.6±0.4
α_{146}			144.8	147.6	146.2±1.4
α_{156}	158.2	154.0	155.7	155.1	155.8±1.5
α_{163}	164.8	163.0	162.8	162.7	163.3±0.9
α_{170}	171.1	168.9	170.0	169.9	170.0±0.8
α_{199}	198.7		198.9		198.8±0.1
α_{205}	204.7		204.6		204.6±0.1
α_{224}	224.2		224.1	224.8	224.4±0.5
α_{240}	239.1	239.2	239.9	239.9	239.5±0.4
α_{272}	272.1	272.5	272.4	273.3	272.6±0.4
α_{290}	290.1		289.2		289.6±0.5
α_{304}	303.6		305.0		304.3±0.7
α_{343}	343.4	341.7	343.3	344.2	343.2±0.6
α_{349}	349.6	348.5	349.3	349.9	349.4±0.5
α_{370}	368.0	369.1	371.3	371.3	369.9±1.4
α_{384}	383.9		384.2	383.0	383.7±0.4
α_{388}	388.2		388.5	388.6	388.4±0.2
α_{394}	392.5		394.2	393.9	393.5±0.7
α_{440}	438.3	439.4	441.1	438.7	439.4±0.7

Table XIII. Abundances of Pa^{228} alpha groups

Alpha group	Abundances (%) Exposure number 148	149	160	161	Adopted
α_0	2.5	2.5	2.0	2.5	2.5
α_{24}	9.1	9.5	10.7	10.9	10.5
α_{38}	12.5	12.8	11.9	11.6	12.0
α_{52}	2.2	2.6	2.1	2.5	2.3
α_{66}	20.1	21.5	20.4	21.2	20.7
α_{77}	1.0		1.3	0.6	1.0
α_{103}	2.3	2.7	2.0	2.3	2.3
α_{116}	8.5	9.0	9.5	8.6	9.0
α_{134}	0.8		0.8	0.7	0.8
α_{146}			0.4	0.2	0.3
α_{156}	1.9	1.1	1.2	0.9	1.1
α_{163}	3.0	2.6	3.0	2.5	2.8
α_{170}	2.9	2.6	2.8	2.5	2.7
α_{199}	0.6		0.6	0.6	0.6
α_{205}	0.6		0.5	0.5	0.5
α_{224}	0.9		0.7	0.9	0.8
α_{240}	1.1		1.1	1.0	1.1
α_{273}	1.6	1.3	1.5	1.3	1.4
α_{290}	0.4		0.2		0.3
α_{304}	0.5		0.4		0.4
α_{343}	7.4	7.9	7.3	7.0	7.3
α_{349}	11.1	11.2	10.9	12.2	11.3
α_{370}	1.4	1.1	1.4	1.5	1.4
α_{384}	2.2	1.9	2.2	1.8	2.0
α_{388}	1.3	1.1	1.4	2.4	1.4
α_{394}	2.7	2.1	2.6	1.8	2.5
α_{440}	1.1	1.0	1.1	1.0	1.0

Table XIV. Alpha groups of Pa^{228}

Alpha-particle energy (Mev)	Excited-state energy (kev)	Abundance (%)	Hindrance factor
6.138	0	2.5	3200
6.114	24.0	10.5	580
6.101	38.1	12.0	350
6.087	52.1	2.3	2000
6.074	66.3	20.7	190
6.062	77.2	1.0	3400
6.037	102.8	2.3	1100
6.024	116.4	9.0	260
6.007	133.6	0.8	2300
5.994	146.2	0.3	5400
5.985	155.8	1.1	1300
5.978	163.3	2.8	480
5.971	170.0	2.7	460
5.943	198.8	0.6	1500
5.937	204.6	0.5	1700
5.918	224.4	0.8	850
5.903	239.5	1.1	520
5.870	272.6	1.4	280
5.854	289.6	0.3	1100
5.839	304.3	0.4	610
5.801	343.2	7.3	24
5.795	349.4	11.3	14
5.775	369.9	1.4	92
5.761	383.7	2.0	55
5.756	388.4	1.4	73
5.752	393.5	2.5	43
5.707	439.4	1.0	57

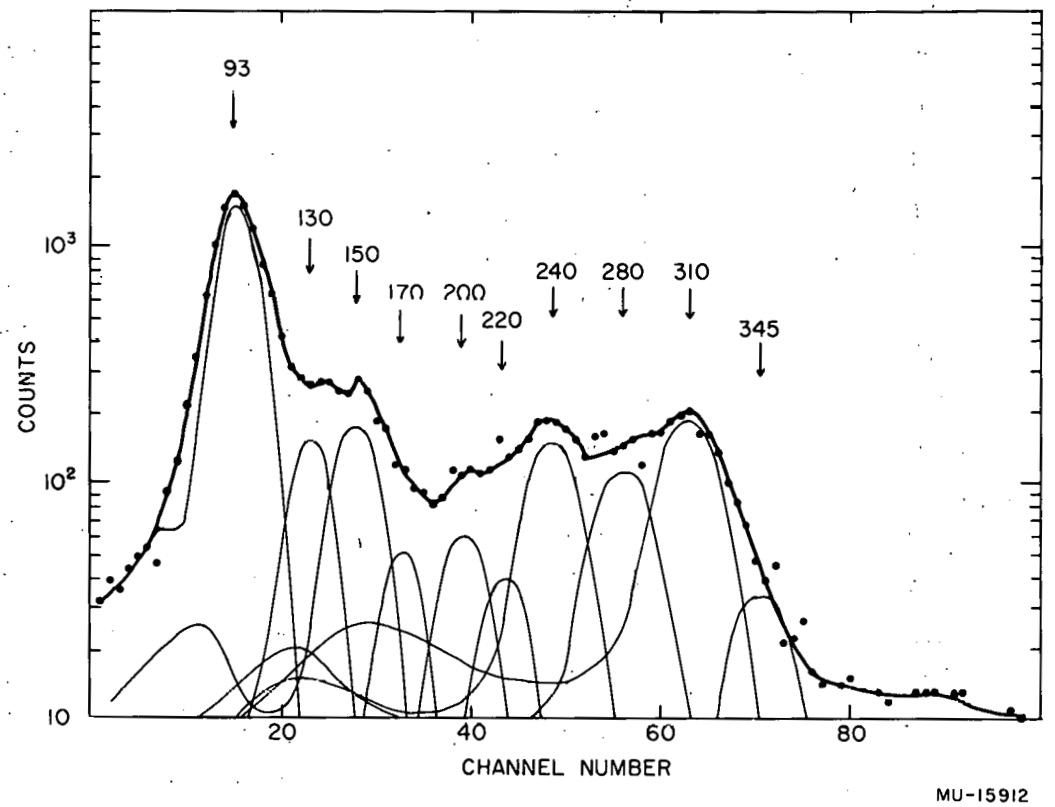

Fig. 15. Alpha particle – gamma ray coincidence spectrum of Pa^{228}.

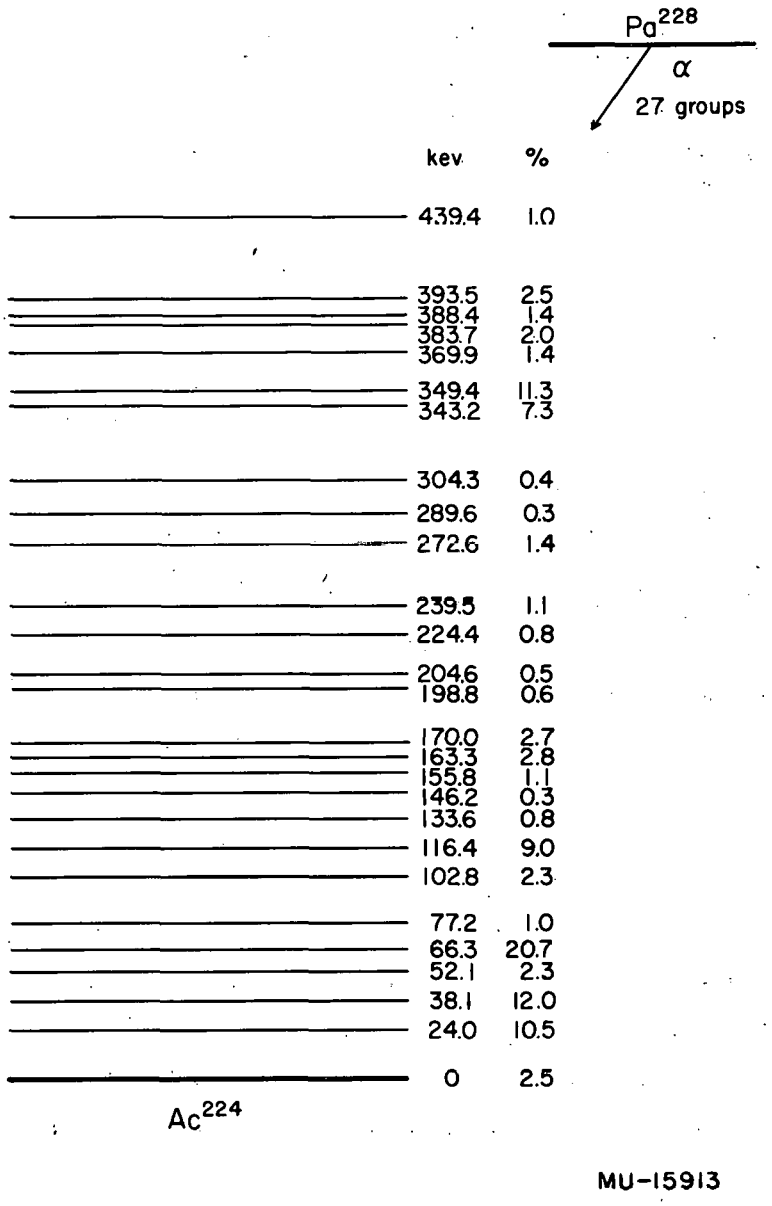

Fig. 16. Alpha decay scheme of Pa^{228}.

be necessary to look for transitions in coincidence with specific alpha groups.

No interpretation can be offered at present concerning the nature and identity of the energy levels in Ac^{224}.

Table XV. Gamma rays in Pa^{228} alpha decay

E_γ (kev)	Relative intensity	E_γ (kev)	Relative intensity
95	240	220	10
130	27	240	55
150	34	280	49
170	11	310	100
200	14	345	21

D. Electron-Capture Decay of Pa^{228}

The electron-capture decay of Pa^{228} has been studied by Passell,[37] who saw transitions of 57.8 and 130 kev, and by Ong Ping Hok,[38] who reported seeing 45 conversion lines and 9 gamma rays corresponding to a total of 18 gamma transitions in Th^{228}. He proposed a decay scheme which incorporated all but two of these transitions.

1. Electron Spectrum

The results of the conversion-electron studies made with the permanent-magnet spectrographs are shown in Table XVI. All these transitions were observed by Ong Ping Hok, with the exception of the 138-kev transition and the Auger transitions. Because of the low transmission of the spectrographs, the weaker lines observed by him were not seen in this study.

The Auger lines served as an excellent energy calibration for the region 65 to 90 kev, and verified the previous calibration of the instruments. The transition energy in the Auger transitions was calculated with the constants of Bergström and Hill.[39] For transitions of the type $K \rightarrow LxMy$, the My binding energies of protactinium were used.

Table XVI. Conversion lines of Pa^{228}

Electron energy (kev)	Relative intensity	Shell	Transition energy (kev)
38.01	vs	L_{II}	57.68
41.39	vs	L_{III}	57.67
52.95	s	M_{II}	57.76
53.71	s	M_{III}	57.74
56.53	m	N_{II}	57.68
56.76	m	N_{III}	57.70
57.54	m	O	57.7
		Adopted value	57.7
109.39	s	L_{II}	129.06
112.80	ms	L_{III}	129.08
124.37	m	M_{II}	129.18
125.09	wm	M_{III}	129.12
128.18	w	N_{II}, N_{III}	129.12
128.99	vw	O	129.2
		Adopted value	129.1
74.88	wm	K	184.51
164.13	vw	L_I	184.58
		Adopted value	184.5
28.26	w	K	137.89
117.61	wm	L_I	138.06
132.91	vw	M_I	138.07
		Adopted value	138.0

Table XVI. Conversion lines of Pa^{228} (cont.)

Electron energy (kev)	Relative intensity	Shell	Transition energy (kev)
114.20	m	K	223.83
203.44	vw	L_I	223.89
		Adopted value	223.8
172.40	w	K	282.03
161.1	vvw	K	270.7
218.0	vvw	K	327.7
299.91	w	K	409.54
68.34	ms	$K \rightarrow L_I\ L_I$	68.34
69.14	ms	$K \rightarrow L_I\ L_{II}$	69.13
72.51	wm	$K \rightarrow L_I\ L_{III}$	72.55
73.30	m	$K \rightarrow L_{II}\ L_{III}$	73.33
76.72	wm	$K \rightarrow L_{III}\ L_{III}$	76.72
83.81	w	$K \rightarrow L_I\ M_I$	83.82
84.15	w	$K \rightarrow L_I\ M_{II}$	84.18
84.97	w	$K \rightarrow L_I\ M_{III}$	85.02
		$K \rightarrow L_{II}\ M_{II}$	84.96
84.61	w	$K \rightarrow L_{II}\ M_I$	84.60
85.83	w	$K \rightarrow L_{II}\ M_{III}$	85.80
88.32	vw	$K \rightarrow L_{III}\ M_{II}$	88.35
89.26	w	$K \rightarrow L_{III}\ M_{III}$	89.19

The relative subshell ratios clearly indicate that the 57.7- and 129.1-kev transitions are E2 in nature, while the 184.5-, 138.0- and 223.8-kev transitions could be either M1 or E1.

2. Gamma Spectrum

Since it is not possible to prepare Pa^{228} in cyclotron bombardments without also producing heavier isotopes, it is necessary to subtract out the contribution from these other isotopes in order to obtain the gamma spectrum of Pa^{228}. This was accomplished in the following manner. The gross gamma spectrum was obtained following a bombardment in which Pa^{228} was produced. The spectrum was observed each day, until all the shorter-lived activities (Pa^{228}, Pa^{229}, Pa^{232}) had decayed out, leaving only the spectrum due to Pa^{230} and Pa^{233}. The latter spectrum was corrected for the decay of Pa^{230} and Pa^{233} back to the time when the first spectrum was recorded. Then a bombardment was made in which no Pa^{228} was produced and the spectrum again obtained. The decay was again followed, and the contribution from Pa^{230} and Pa^{233} was obtained. By normalizing the two spectra to the same Pa^{230},Pa^{233} background, it was then possible to obtain the contribution of Pa^{229}, Pa^{230}, Pa^{232}, and Pa^{233} to the gross gamma spectrum. The difference then gives the spectrum of Pa^{228}.

Figures 17 through 21 show the spectra obtained in this manner for three different energy regions. The energies and relative intensities of the gamma rays are listed in Table XVII. Lead absorber was used in each case to reduce the intensity of thorium K x-rays. The x-ray peak observed in each spectrum is thus almost exclusively due to lead K x-rays which were induced by this absorption. The intensities of the thorium K x-rays were calculated from spectra obtained with no absorber. Although the higher-energy gamma rays (> 1 Mev) were seen in quite low intensity, they are definitely real and belong to Pa^{228}. Their decay was followed for about four half lives, and since the other isotopes of protactinium have no gamma rays in this energy region, the assignment is unambiguous. Of course, the resolution of the curves is subject to the usual errors inherent in such a method.

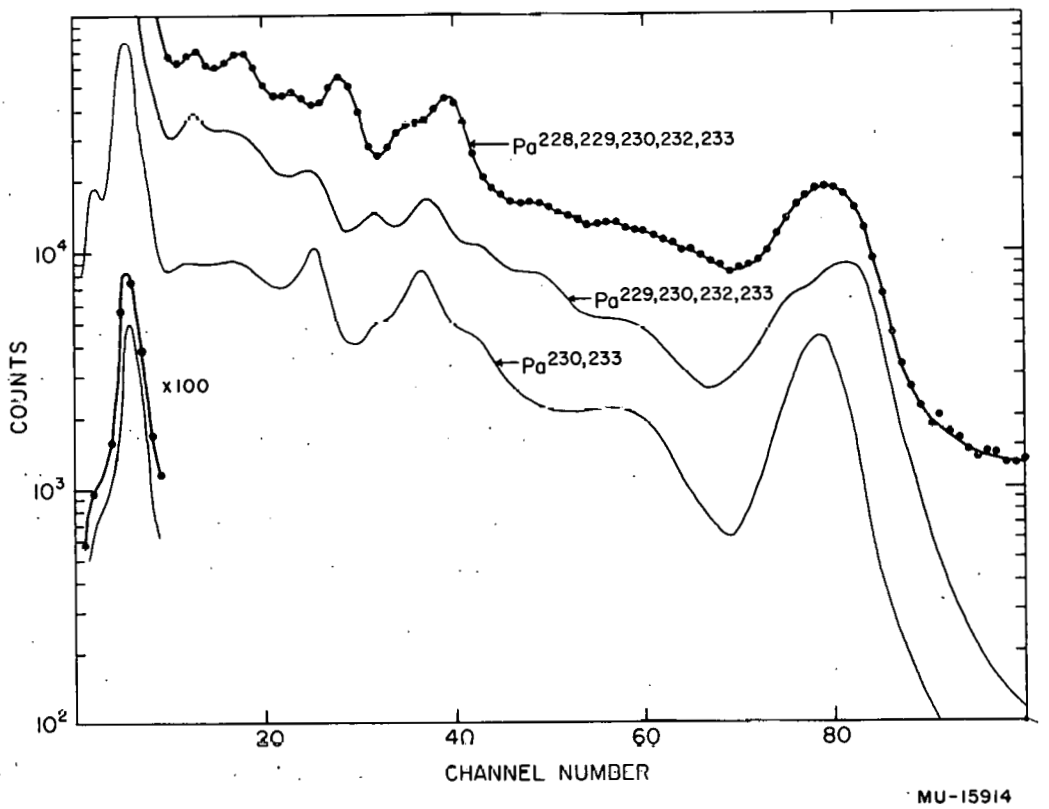

Fig. 17. Gamma-ray spectra of protactinium isotopes, 0 to 1300 kev — 522 mg/cm^2 Pb absorber.

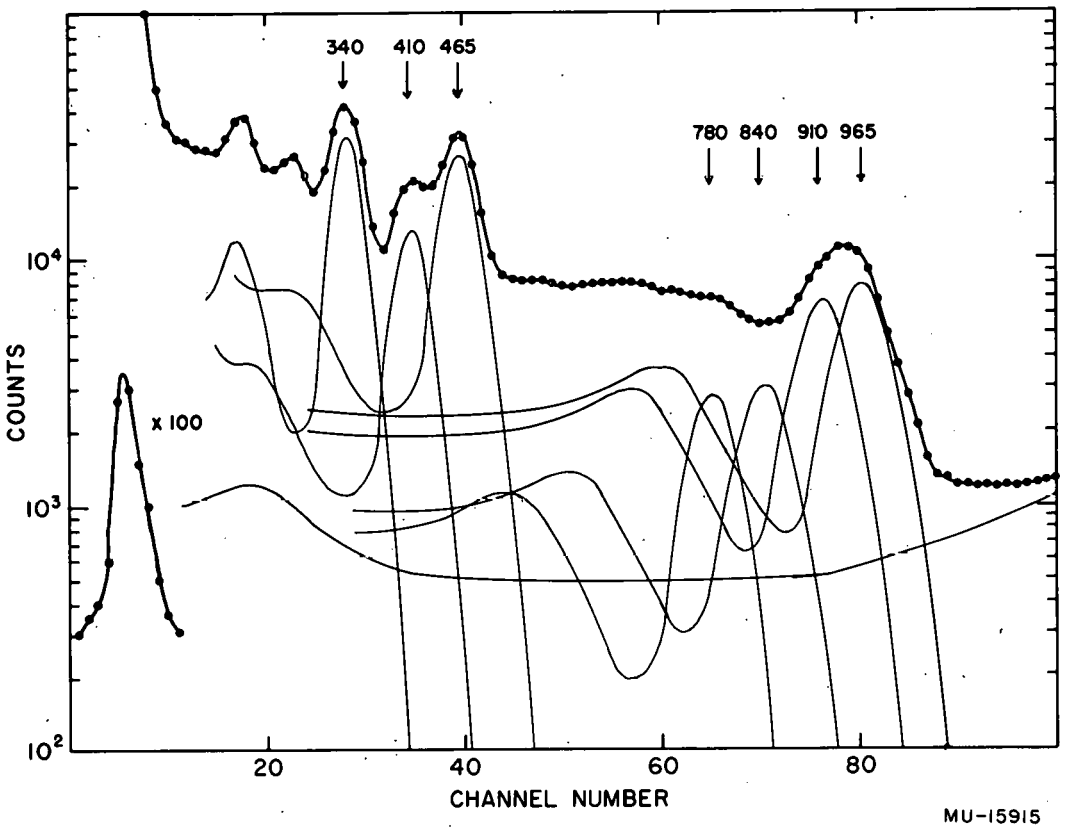

Fig. 18. Gamma-ray spectrum of Pa^{228}, 0 to 1300 kev—522 mg/cm^2 Pb absorber.

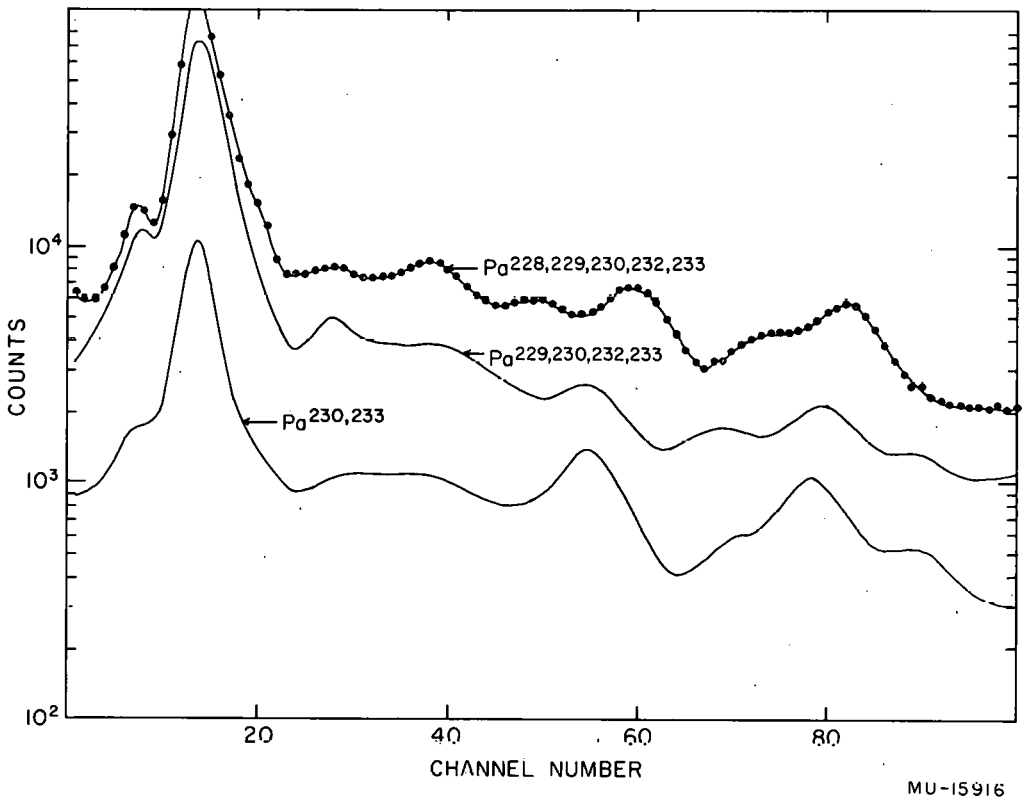

Fig. 19. Gamma-ray spectra of protactinium isotopes, 0 to 500 kev—522 mg/cm^2 Pb absorber.

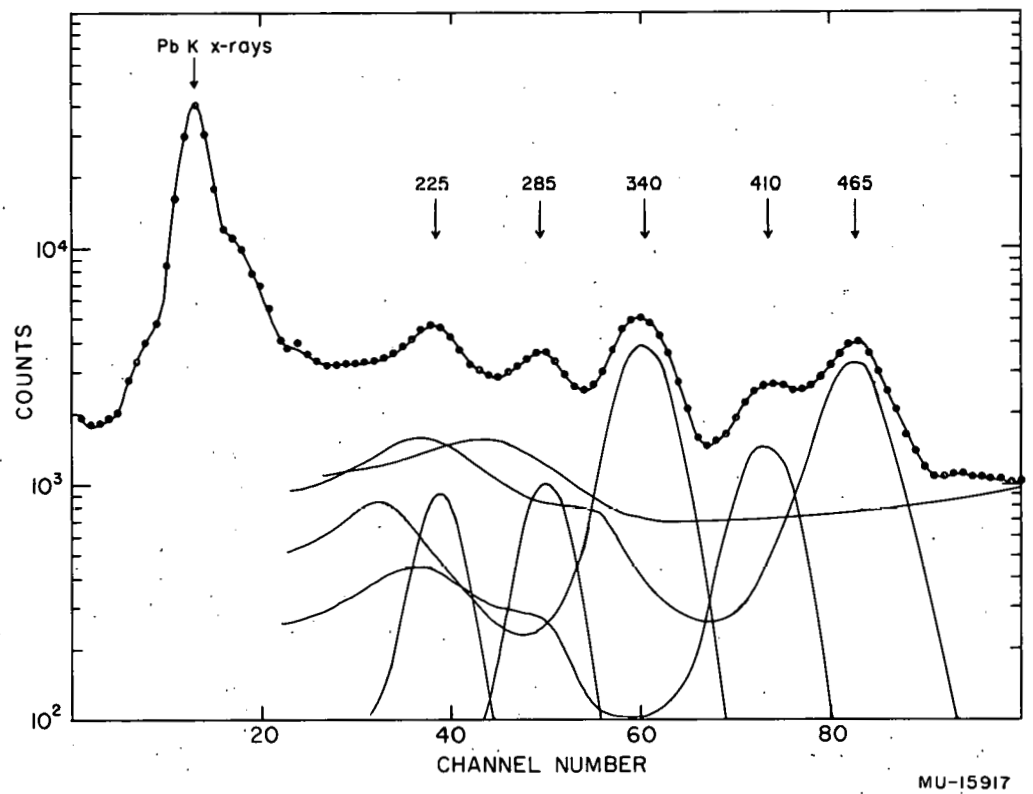

Fig. 20. Gamma-ray spectrum of Pa^{228}, 0 to 600 kev—522 mg/cm^2 Pb absorber.

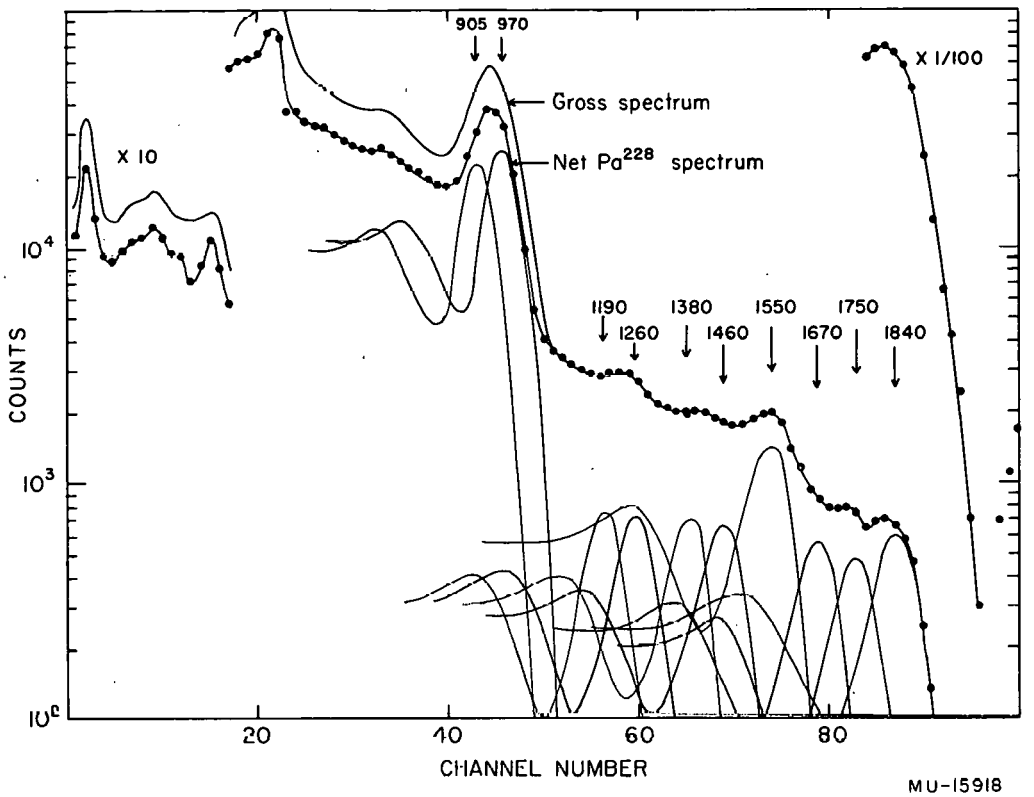

Fig. 21. High-energy gamma-ray spectrum of Pa^{228}—1471 mg/cm^2 Pb absorber.

The intensities of the gamma rays agree reasonably well with those found by Ong Ping Hok, although there are some discrepancies. It is of interest to note that many of the same transitions were observed by Box and Klaiber in their scintillation studies of the beta decay of Ac^{228},[40] although the intensities are considerably different in many cases. The transitions of ~450 kev are much weaker in Ac^{228} decay, while the 225- and 340-kev transitions are much stronger.

Table XVII. Gamma rays of Pa^{228}

E_γ (kev)	Relative intensity	E_γ (kev)	Relative intensity
225	70	1190	45
285	88	1260	48
340	510	1380	53
410	300	1460	54
465	880	1550	105
780	230	1670	56
840	290	1750	50
900	770	1840	70
965	1000	thorium K x-rays	6000

Gamma-gamma coincidence studies were also made, although the results were rather inconclusive. They did indicate that the 465-kev photons were in coincidence with both the 910- and 965-kev transitions, slightly favoring the former. The 410-kev photons, on the other hand, favored the higher-energy 965-kev transition. The 780-kev gamma ray appeared to be in coincidence with 340-kev photons.

3. Decay Scheme

The electron-capture decay scheme of Pa^{228} is shown in Fig. 22. All the transitions listed in Tables XVI and XVII are placed with the exception of the weak 1750-kev gamma ray. The dotted 97-kev transition was not observed in this study, but was seen by Ong Ping Hok. The

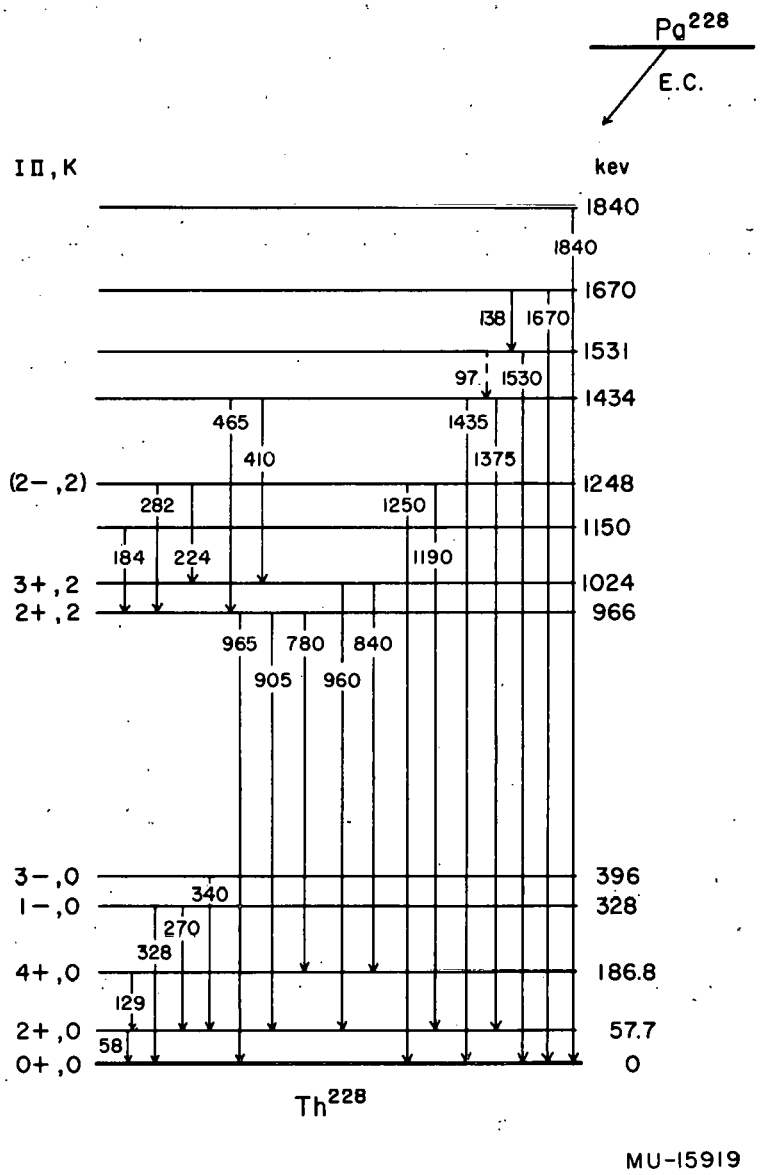

Fig. 22. Electron-capture decay scheme of Pa^{228}.

energies and assignments of the lower levels are fairly certain, while those at higher energies (above 1100 kev) are very tentative and uncertain.

This decay scheme differs considerably from that of Ong Ping Hok,[18] but is similar in many respects to that of Bjornholm et al.[41] The major differences occur in the levels above 1100 kev.

In addition to the ground-state rotational band with its even and odd parity members, there is a gamma vibrational band at about 1 Mev. The 2+, 3+, and possibly 2- members of this band are observed, although the assignment of the last is subject to question. The assignment was based on the energy difference between the 282.0- and 223.8-kev transitions observed with the permanent-magnet spectrographs. This energy difference of 58.2 kev is not the same as the energy separation between the ground and first excited states, although it differs by only 0.5 kev. Since the energy separation of the first two members of the gamma vibrational band is expected to be of similar magnitude, the transitions are assumed to populate these levels. Although the multipolarities of these transitions are not known, they are assumed to be E1, in analogy with the E1 transitions from the 1- state of the ground-state rotational band. Little can be said of the spins and parities of the higher excited states.

The similarity of this decay to that of Ac^{228} suggests that the spin of Pa^{228} is within ± 1 of that of Ac^{228}, which is thought to be 2 or 3. Since it appears that the 3- state at 396 kev is populated to a much greater extent in Ac^{228} decay, assignments of $I = 2$ for Pa^{228} and $I = 3$ for Ac^{228} would not be unreasonable. According to Moszkowski[42] the spin and parity of an odd-odd nuclide may be predicted from a knowledge of the intrinsic states of the odd proton and neutron which couple together to give the resultant spin and parity of the nuclide in question. In Pa^{228}, the intrinsic states of the 91st proton and 137th neutron are needed. The proton in Pa^{229} has already been assigned 5/2- (523)↓ (Section III-A.4), the arrow pointing down indicating that the intrinsic spin of the odd nucleon ($S = 1/2$) must be subtracted from Λ (= 3) to give $I = 5/2$. The most likely assignment for the 137th neutron on the

Nilsson diagram would be 3/2+ (631)↑. Moszkowski's rule predicts very simply that if the arrows both point in the same direction, the resultant spin is given by |Ip + In|; if in opposite directions, by |Ip - In|. This would predict a spin of 1- for Pa^{228}.

E. Alpha Decay of Pa^{227}

Pa^{227} was shown by Meinke to decay 85% by alpha-particle emission and 15% by electron capture, with a total half life of 38.3 min.[17] The energy of the alpha particles was determined as 6.46 Mev.

1. Alpha Spectrum

Pa^{227} was prepared by bombarding thorium metal with minimum-energy (280-Mev) protons at the 184-inch cyclotron. Its alpha spectrum was obtained with the double-focusing spectrograph using a sample containing 1.4×10^8 alpha disintegrations per minute, with a defining slit of 0.010 inch and baffle openings of 3.0 cm. The alpha spectrum is shown in Fig. 23, and the data are summarized in Table XVIII. These data were based on two spectra which were obtained while following the decay of the peaks. The excited state energies should be good to ± 0.5 kev, and the abundances to about 5%.

Table XVIII. Pa^{227} Alpha Groups

Alpha-particle energy[a] (Mev)	Excited-state energy (kev)	Abundance (%)	Hindrance factor
6.526	0	2.3	130
6.515	10.7	0.3	900
6.460	67.3	49.5	3.1
6.418	109.7	11.5	8.8
6.410	117.8	14.8	6.3
6.396	132.0	9.3	8.8
6.371	157.9	2.6	24
6.351	177.6	7.8	6.6
6.331	198.6	0.7	60
6.321	208.6	0.4	95
6.294	235.6	0.8	36

[a] Relative to $Bi^{211}_{\alpha_{354}}$ = 6.273 Mev.

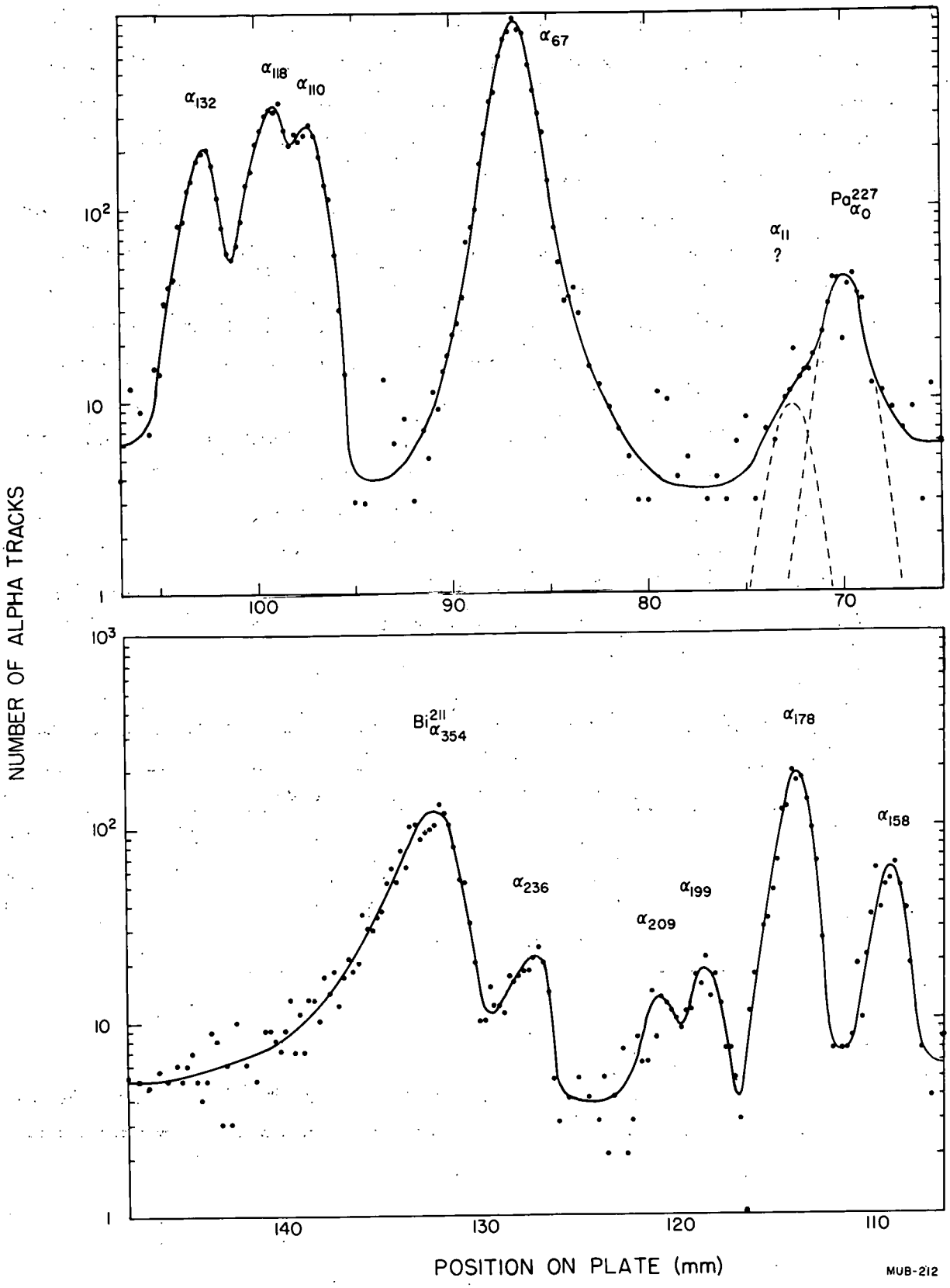

Fig. 23. Alpha-particle spectrum of Pa^{227}—double-focusing spectrograph.

2. Decay Scheme and Interpretation of Levels

The alpha decay scheme of Pa^{227} is shown in Fig. 24. Although alpha-gamma coincidences were looked for, the results were very inconclusive. A 67-kev transition was seen in an intensity which would indicate that it was probably not entirely due to platinum K x-rays. However, the decay scheme was constructed by using only the alpha-particle energies and abundances.

Certain features of the decay scheme are similar to those of Pa^{229}, while others are not. The alpha group leading to the ground state is hindered to a much greater extent in Pa^{227}, while the hindrance factors to higher states are much smaller. In each case, a low hindrance factor indicating "favored" alpha decay to one level is observed.

The levels at 67.3, 109.7, 157.9, and 208.6 kev are interpreted as being members of a K = 5/2 rotational band with the Nilsson assignment 5/2- (523). In this case, however, the energies of the levels deviate somewhat from the simple I (I+1) dependence, and an additional term of the form $BI^2 (I+1)^2$ must be added. Table XIX compares the experimental energies and intensities with those calculated using Eqs. (3) and (4). The agreement is quite satisfactory.

Table XIX. Favored alpha decay to K = 5/2 band in Ac^{223}

Spin of state	Excited State Energy (kev)			Rel. Int.	
	Exp.	Theor.(Simple)[a]	Theor.(I^2Term)[b]	Exp.	Theor.[c]
5/2	67.3	(67.3)	(67.3)	100	(100)
7/2	109.7	(109.7)	(109.7)	23	20
9/2	157.9	164.2	(157.9)	5.3	6.3
11/2	208.6	230.9	209.5	0.8	1.2

[a] $\hbar^2/2\Im$ = 6.06 kev

[b] $\hbar^2/2\Im$ = 7.18 kev, B = -0.045 kev

[c] C_0 = 1.00, C_2 = 0.77, C_4 = 0.19 (From Th^{226} hindrance factors)

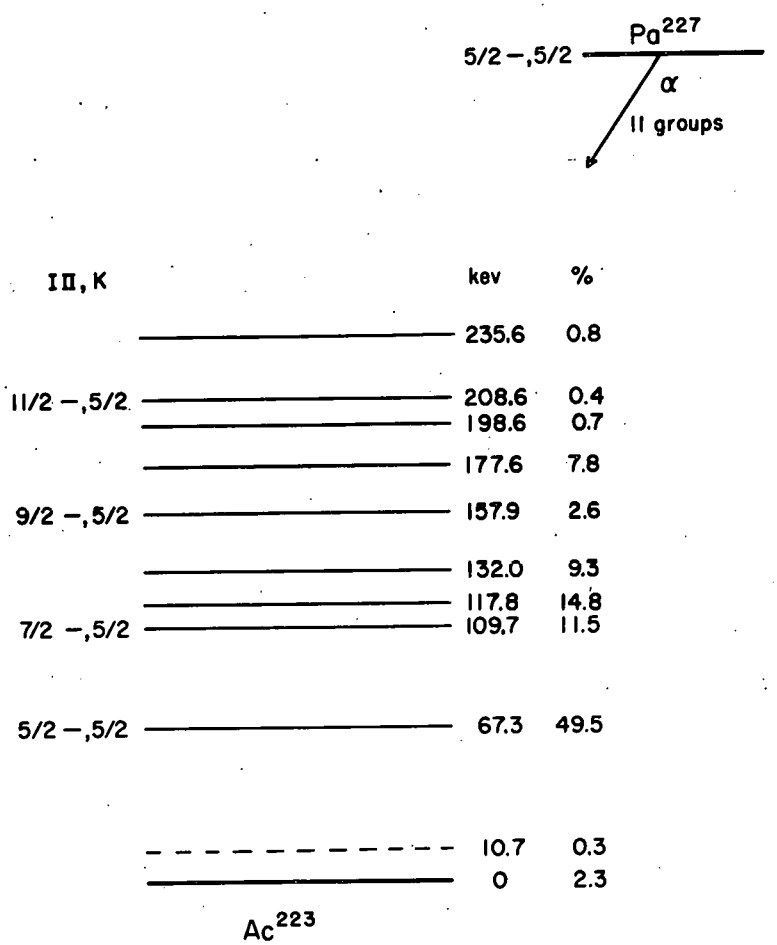

Fig. 24. Alpha decay scheme of Pa^{227}.

A search for a second K = 5/2 band analogous to that in Ac^{225} reveals that the levels at 132.0, 177.6, and 235.6 kev give good agreement with the expected energy-level spacings. However, the intensities give very poor agreement with theory, the upper level receiving far too much population and the second level far too little.

At the deformation expected for Ac^{223}, the 1/2- (530) state is found at slightly higher excitation than the 5/2- (523) state, which is assigned to the rotational band based on the level at 67.3 kev. In view of the fact that the asymptotic quantum numbers of these two states are similar, the hindrance factors might be expected to be of the same order of magnitude. This would explain the relatively low hindrance factors of some of the higher excited states. However, even though the energy-level spacings of several of these levels can be matched reasonably well by adjustment of the parameters in Eq. (3) for a K = 1/2 band, the relative populations cannot be made to give satisfactory agreement. Use of odd-L alpha waves likewise fails to give agreement.

Because of the lack of further information concerning the internal transitions in Ac^{223}, and the failure of theory to match the experimental alpha-decay pattern, the identity of the remaining levels remains unsettled.

F. Electron-Capture Decay of Pa^{230}

Pa^{230} decays 92% by electron capture and 8% by beta emission, with a total half life of 17 days.[44] Meinke also reports a weak alpha branching of 0.003%.[17] The radiations have been studied by Passell[37] and by Ong Ping Hok,[45] who observed the electron lines and gamma rays of 11 transitions. He proposed two possible decay schemes.

1. Electron Spectrum

The results of the conversion-electron studies made with the permanent-magnet spectrographs are shown in Table XX. Only the transitions of 52.2, 120.8, 228.0, and 443.6 kev may be assigned with confidence to the electron-capture decay of Pa^{230}. Some of the other lines

Table XX. Conversion lines of Pa^{230}

Electron energy (kev)	Relative intensity		Sub-shell	Transition energy (kev)
33.45	vvs	32	L_{II}	53.12
36.89	vvs	33	L_{III}	53.17
48.37	vs	13	M_{II}	53.18
49.14	vs	13	M_{III}	53.17
52.05	ms	6	N_{II}	53.10
52.14	ms		N_{III}	53.08
52.89	m	1.4	O	53.1
			Adopted value	53.15
101.08	s	2.3	L_{II}	120.75
104.49	s		L_{III}	120.77
116.09	m		M_{II}	120.90
116.83	m		M_{III}	120.86
119.73	w		N_{II}	120.88
			Adopted value	120.8
118.38	ms	0.4	K	228.01
207.41	w		L_{I}	227.86
			Adopted value	228.0
333.95	ms		K	443.58
423.19	wm		L_{I}	443.64
			Adopted value	443.6
338.3	vw			
345.1	vw			
353.7	wm			
376.4	vvw			
430.0	vvw			
515.5	vw			
526.3	vw			

may be due to transitions in U^{230} following beta decay, although the disintegration energy is only 410 kev.[45] They are shown in Table XX only because the E.C./β^- ratio is so large. The electron lines listed, even though some are weak, have consistently appeared on several plates following different bombardments.

The 53.2- and 120.8-kev transitions are both E2, while the multipolarities of the other transitions are unassigned.

2. Gamma Spectrum

Figure 25 shows the gamma spectrum of Pa^{230} and Pa^{233}, both of which were formed in the bombardments. The spectrum due to Pa^{233} was obtained by using isotopically pure Pa^{233} produced by neutron irradiation of thorium metal. The difference between the curves, representing the Pa^{230} contribution, is shown in Fig. 26. The energies and relative abundances of the gamma rays are summarized in Table XXI. It is assumed that the gamma rays follow the electron-capture decay of Pa^{230}, although this may not be justified.

Table XXI. Gamma rays of Pa^{230}

E_γ (kev)	Relative intensity	E_γ (kev)	Relative intensity
275	35	905	620
400	105	945	1000
450	460	1060	44
510	220	K x-rays	2300
560	70		

Alpha-gamma coincidence studies revealed that the 400 to 510 kev gamma rays are not in coincidence with the 940-kev photons, in contrast to the decay of Pa^{228}. Since the E.C. disintegration energy is expected to be only 1240 kev,[46] this is not surprising. Coincidence techniques failed to resolve the complex group around 450 kev.

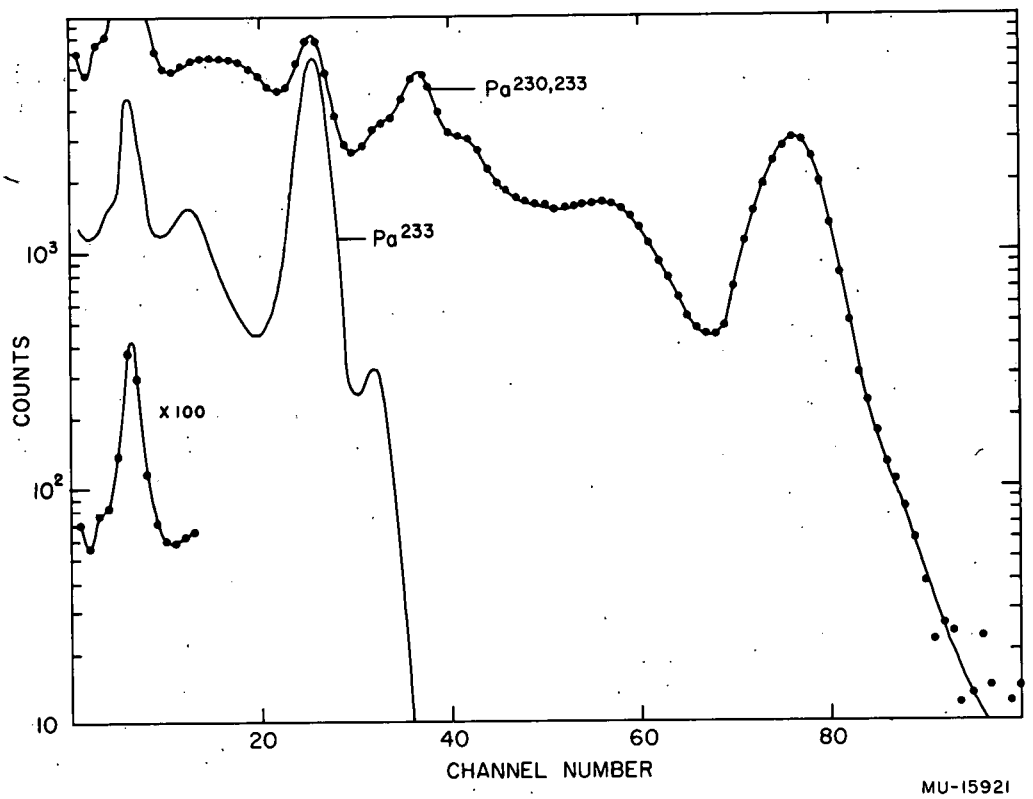

Fig. 25. Gamma-ray spectra of Pa^{230} and Pa^{233} — 728 mg/cm^2 Pb absorber.

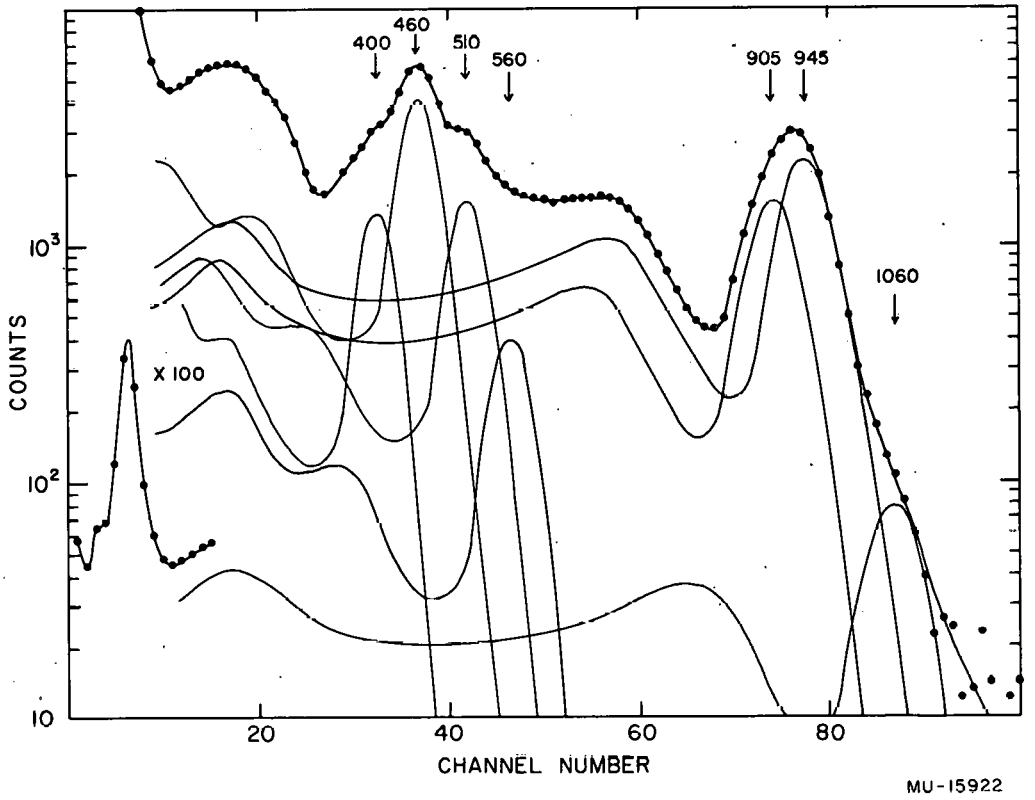

Fig. 26. Gamma-ray spectrum of Pa^{230} —728 mg/cm^2 Pb absorber.

3. Decay Scheme and Interpretation of Levels

A decay scheme which incorporates some, but not all, of the transitions is shown in Fig. 27. As the multipolarities of most of the transitions are unknown, only the spins and parities of the first three members of the ground-state rotational band are assigned with certainty.

The 1- state at 505 kev is based on gamma rays of 510 and 450 kev. These gamma rays were also observed following the alpha decay of U^{234}.[47]

The level at 950 kev is assigned as the 2+ member of the gamma vibrational band in analogy to the 966-kev level in Th^{288} (Fig. 22). However, the complex peak at 940 kev in the gamma spectrum is much narrower than the complex peak observed in Pa^{228} decay, and the best resolution gives gamma rays of 905 and 945 kev.

The decay scheme is undoubtedly much more complex than that shown in Fig. 29, since there are so many transitions that have not been placed. However, a satisfactory decay scheme cannot be proposed without additional information.

G. Beta Decay of Pa^{230}

Prior to this study, nothing was known about the excited states of U^{230}.[46] Ong Ping Hok and Passell both failed to observe any transitions that might be ascribed to the beta decay of Pa^{230}.

1. Electron Spectrum

Table XXII summarizes the data obtained with the permanent-magnet spectrographs. The conversion lines of only one transition in U^{230} were observed. This E2 transition undoubtedly proceeds from the first excited state to ground.

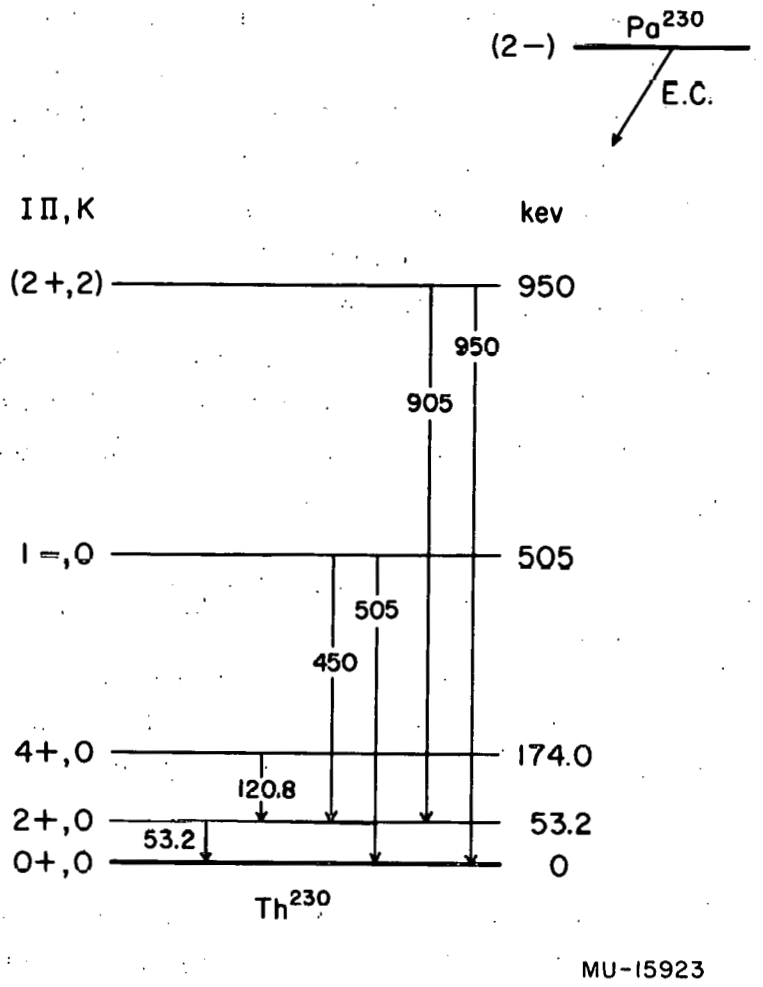

Fig. 27. Electron-capture decay scheme of Pa^{230}.

Table XXII. Conversion lines in Pa^{230} beta decay

Electron energy (kev)	Relative intensity		Sub-shell	Transition energy (kev)
30.72	ms	4	L_{II}	51.66
34.52	ms	5	L_{III}	51.68
46.49	m		M_{II}	51.67
47.39	m		M_{III}	51.69
50.38	w		N_{II}	51.65
50.59	w		N_{III}	51.63
				51.67

2. Decay Scheme and Interpretation of Levels

Figure 28 shows the beta decay scheme of Pa^{230}. Since the branching ratio to the two levels is unknown, only the transition to the upper state is shown. These two levels are assumed to be the 0+ and 2+ members of the ground-state rotational band, by analogy with the many others observed in this region. The 2+ level at 51.7 kev is assumed to be directly populated by beta decay, since no other internal transitions were observed and the only other levels expected below 410 kev would be the 4+ and 6+ members of the ground-state rotational band.

The 91st proton in Pa^{231} is given the Nilsson assignment 1/2- (530)↑, and in Pa^{229} 5/2- (523)↓. The 139th neutron in Th^{229} is assigned 5/2+ (633)↓. By Moszkowski's rules the spin and parity of Pa^{230} should then be either 2- or 5-. The fact that beta decay takes place to the 2+ level in U^{230} would favor the choice of 2-, especially since no population to the 4+ or higher levels is observed.

H. Beta Decay of Pa^{232}

Pa^{232} decays by beta emission with a half life of 1.3 days.[46] The beta and gamma spectra have been studied quite extensively by Ong Ping Hok[18,48] and by Browne et al.[49] The latter group found three beta components and 15 gamma rays (energies and intensities not published), while

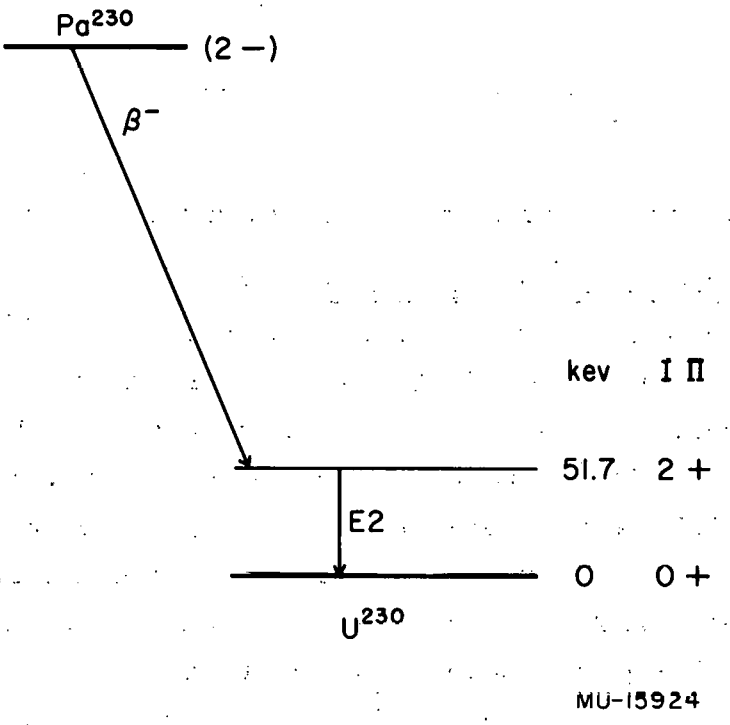

Fig. 28. Beta decay scheme of Pa^{230}.

Ong Ping Hok found four beta components and 16 gamma transitions. He also proposed a decay scheme.

Since Pa^{232} was produced only as a by-product in these bombardments, no extensive studies were made of its radiations. The following results were obtained during studies concentrated on the lighter isotopes of protactinium.

1. Electron Spectrum

Table XXIII summarizes the electron data obtained with the permanent-magnet spectrographs. Only the very intense lines observed by Ong Ping Hok were seen. It appears that the multipolarity of each of these transitions is E2.

2. Gamma Spectrum

The spectra of a sample containing Pa^{229}, Pa^{232}, Pa^{230}, and Pa^{233} are shown in Figs. 17 and 19. The spectra due to the latter two isotopes alone are also shown. The difference, representing the gamma spectrum of Pa^{229} and Pa^{232}, is shown in Fig. 29. In addition to the gamma rays resolved from this spectrum, one of 1150 kev appeared in the higher-energy region. The energies and relative abundances of the gamma rays are shown in Table XXIV. Most of the x-rays are due to the electron-capture decay of Pa^{229}, while all of the gamma rays are assigned to Pa^{232} decay.

Table XXIV. Gamma rays of Pa^{232}

E_γ (kev)	Relative abundance	E_γ (kev)	Relative abundance
155	240	845	185
390	160	900	410
455	250	980	1000
515	140	1150	50
575	140	K x-rays	5300

Table XXIII. Conversion lines of Pa^{232}

Electron energy (kev)	Relative intensity		Sub-shell	Transition energy (kev)
26.55	vs	32	L_{II}	47.49
30.33	vs	33	L_{III}	47.49
42.33	ms	21	M_{II}	47.51
43.17	ms	15	M_{III}	47.47
46.19	m	11	N_{II}	47.46
46.43	m		N_{III}	47.47
47.33	wm	4	O	47.5
			Adopted value	47.48
87.94	s	18	L_{II}	108.88
91.74	s	13	L_{III}	108.90
103.72	m	6	M_{II}	108.90
104.50	m	6	M_{III}	108.80
107.59	w	3	N_{II}	108.86
107.81	w		N_{III}	108.85
108.59	w		O	108.8
			Adopted value	108.9
272.15	vw		K	387.74
365.91	vw		L_{I}	387.67
			Adopted value	387.7

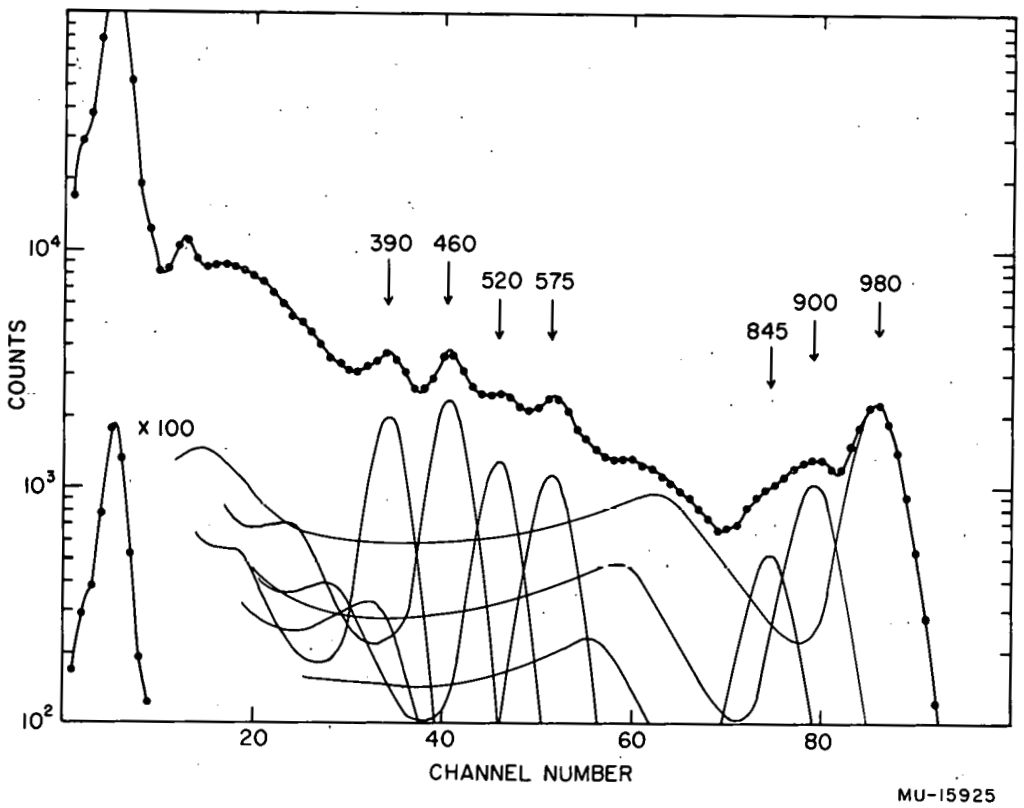

Fig. 29. Gamma ray spectrum of Pa^{232}—522 mg/cm^2 Pb absorber.

3. Decay Scheme and Interpretation of Levels

A decay scheme which utilizes nearly all the observed transitions is shown in Fig. 30. Transition energies shown in Table XXIII were used where applicable, and those obtained by Ong Ping Hok were used elsewhere. This decay scheme differs from his in only one respect -- the order of the 517-455 cascade is reversed, since the latter is more intense.

The spins and parities of the ground-state rotational band are the only ones that may be assigned with confidence. The levels at 388 and 455 kev were based on the close agreement between the sums of the gamma-ray pairs and the cross-over transition of 972 kev. Their identity is unknown.

The level at 868 kev may be the 2+ base member of a gamma vibrational band, although this is not certain.

Ong Ping Hok assumes a spin and parity of 2- for Pa^{232} in order to fit his log (ft) values. This would be in perfect agreement with the prediction based on Moszkowski's rules, using 1/2- (530)↑ for the 91st proton in both Pa^{231} and Pa^{233} and 5/2+ (633)↓ for the 141st neutron in both Th^{231} and U^{233}.

I. Beta Decay of Pa^{233}

Pa^{233} is a 27-day beta emitter whose radiations have been extensively investigated.[46] It is especially noted for the very large number of conversion electrons emitted in its decay.

In bombardments of Th^{230}, ^{232} with deuterons or of Th^{232} with protons, one would not expect to make appreciable quantities of Pa^{233}. However, in each type of bombardment, large amounts of Pa^{233} were formed, presumably by the $Th^{232}(n,\gamma)Th^{233}$ reaction, followed by the 23-min beta decay of Th^{233} to Pa^{233}. The following results were also obtained during experiments concentrated on the lighter isotopes of protactinium.

1. Electron Spectrum

The conversion lines of Pa^{233} obtained with the permanent-magnet spectrographs are shown in Table XXV. Although little can be said about the multipolarities of many of the transitions, assignments of E2-M1 would not be inconsistent with the observed patterns.

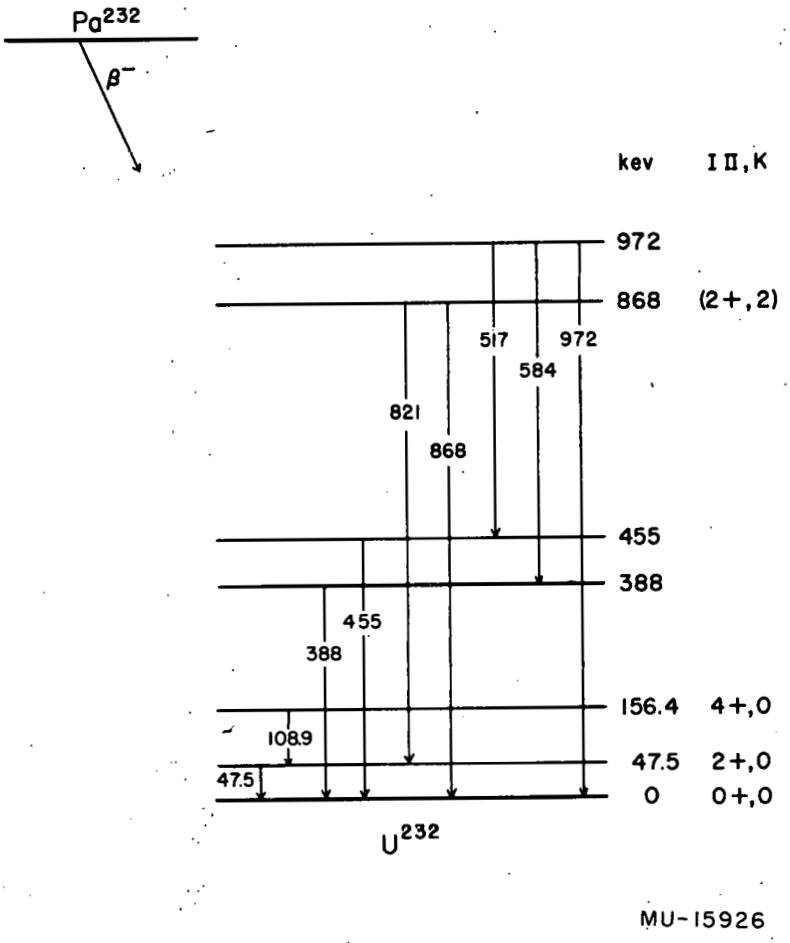

Fig. 30. Decay scheme of Pa^{232}.

Table XXV. Conversion lines of Pa^{233}

Electron energy (kev)	Relative intensity		Sub-shell	Transition energy (kev)
19.32	w		L_{II}	40.26
23.11	w		L_{III}	40.27
35.09	vw		M_{II}	40.27
39.02	vvw		N_{II}	40.29
			Adopted value	40.27
53.36	ms	3	L_I	75.12
54.22	wm		L_{II}	75.16
69.64	m	1	M_I	75.19
73.70	wm		N_I	75.14
74.71	vw		O	75.0
			Adopted value	75.15
64.67	s	4	L_I	86.43
65.47	m	1	L_{II}	86.51
80.95	ms	1	M_I	86.50
81.31	vvw		M_{II}	86.47
85.08	wm		N_I	86.52
			Adopted value	86.49
82.01	ms	0.8	L_I	103.77
82.80	w		L_{II}	103.74
98.22	wm		M_I	103.77
102.27	vw		N_I	103.71
			Adopted value	103.8

Table XXV. Conversion lines of Pa^{233} (cont.)

Electron energy (kev)	Relative intensity		Sub-shell	Transition energy (kev)
184.42	vs	2.3	K	300.01
278.29	s		L_I	300.05
294.33	m		M_I	299.88
			Adopted value	300.0
196.08	vvs	10	K	311.67
289.89	vs		L_I	311.65
305.98	m		M_I	311.53
310.06	w		N_I	311.50
			Adopted value	311.6
224.75	ms		K	340.34
318.56	w		L_I	340.32
			Adopted value	340.3
299.95	m		K	415.54
393.78	w		L_I	415.54
			Adopted value	415.5

2. Gamma Spectrum

The gamma spectrum of Pa^{233} is shown in Fig. 31. No attempt has been made to resolve the peaks, since they are known to be composed of several components of approximately the same energy.

3. Decay Scheme and Interpretation of Levels

The decay scheme of Pa^{233} is shown in Fig. 32. It is identical to that proposed by Ong Ping Hok[18] and earlier by Brodie,[50] with the exception of the energies, which were taken from this work. The transitions that were observed by Ong Ping Hok but were too weak to be seen in this study are shown by dotted lines, with the energies obtained by difference. The abundances of the beta components were also taken from Ong Ping Hok.

The Nilsson assignments were proposed by Newton,[35] and are consistent with the decay scheme shown.

J. Electron-Capture Decay of Ac^{224}

Ac^{224} decays 90% by electron capture and 10% by alpha-particle emission, with a total half life of 2.9 hours.[17] Since it may be easily obtained by a milking experiment from Pa^{228}, it was felt advisable to investigate its electron-capture decay to Ra^{224}. The low-lying levels in Ra^{224} had been previously studied by Stephens[51] following the alpha decay of Th^{228}. Figure 33 shows the decay scheme of Th^{228}.

1. Gamma Spectrum

The singles gamma spectrum of Ac^{224} as well as the K x-ray–gamma coincidence spectrum showed only K x-rays and gamma rays of 133 and 217 kev. A typical gamma-ray spectrum is shown in Fig. 34. A search for higher-energy gamma rays revealed none, although the total disintegration energy is estimated to be 1370 kev.[46] An upper limit of 2% was set for the intensity of any gamma ray above 220 kev. Figure 35 shows the high-energy gamma spectrum.

Since only K x-rays and gamma rays of 133 and 217 kev appeared, it is obvious that decay is taking place to the 1- level in Ra^{224}. The

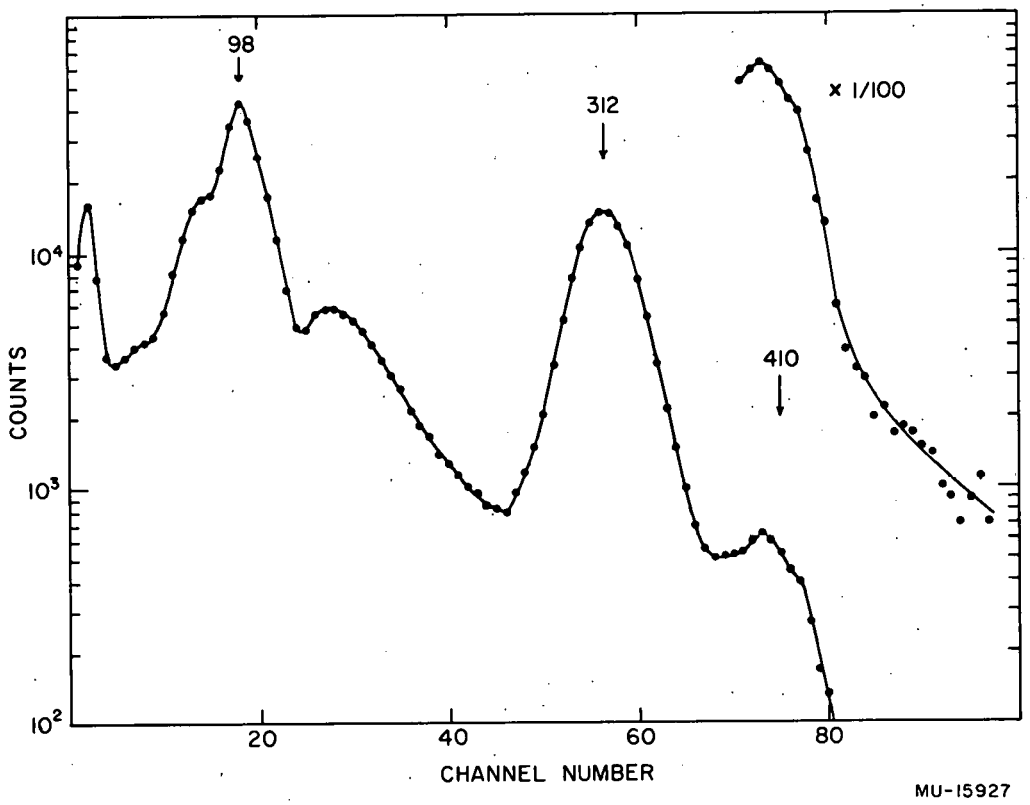

Fig. 31. Gamma-ray spectrum of Pa^{233}.

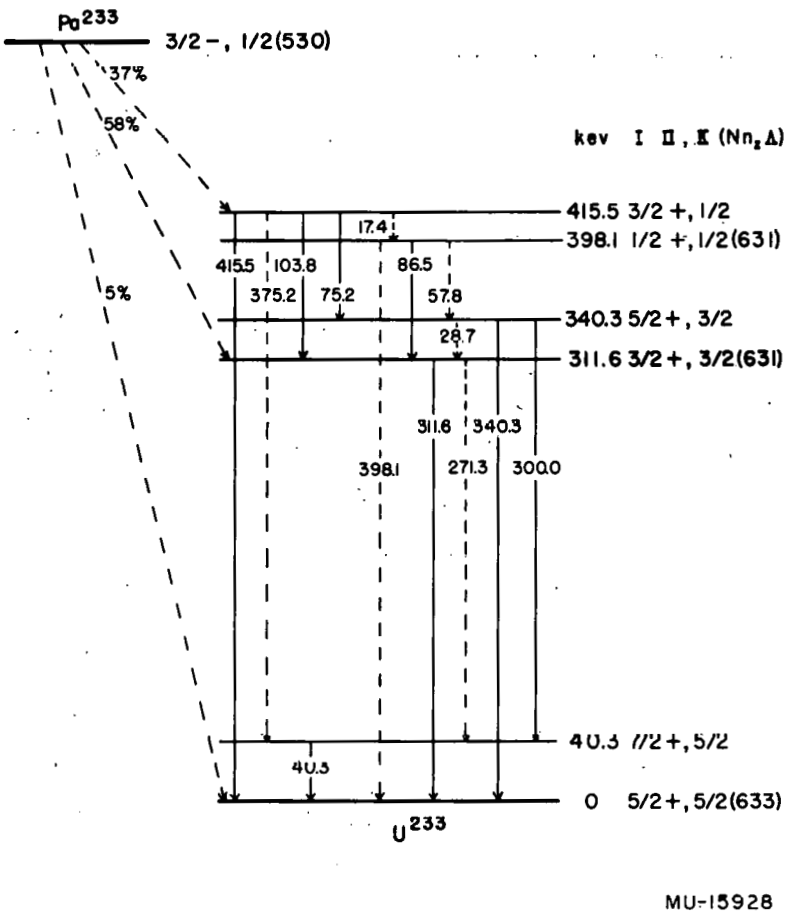

Fig. 32. Decay scheme of Pa^{233}.

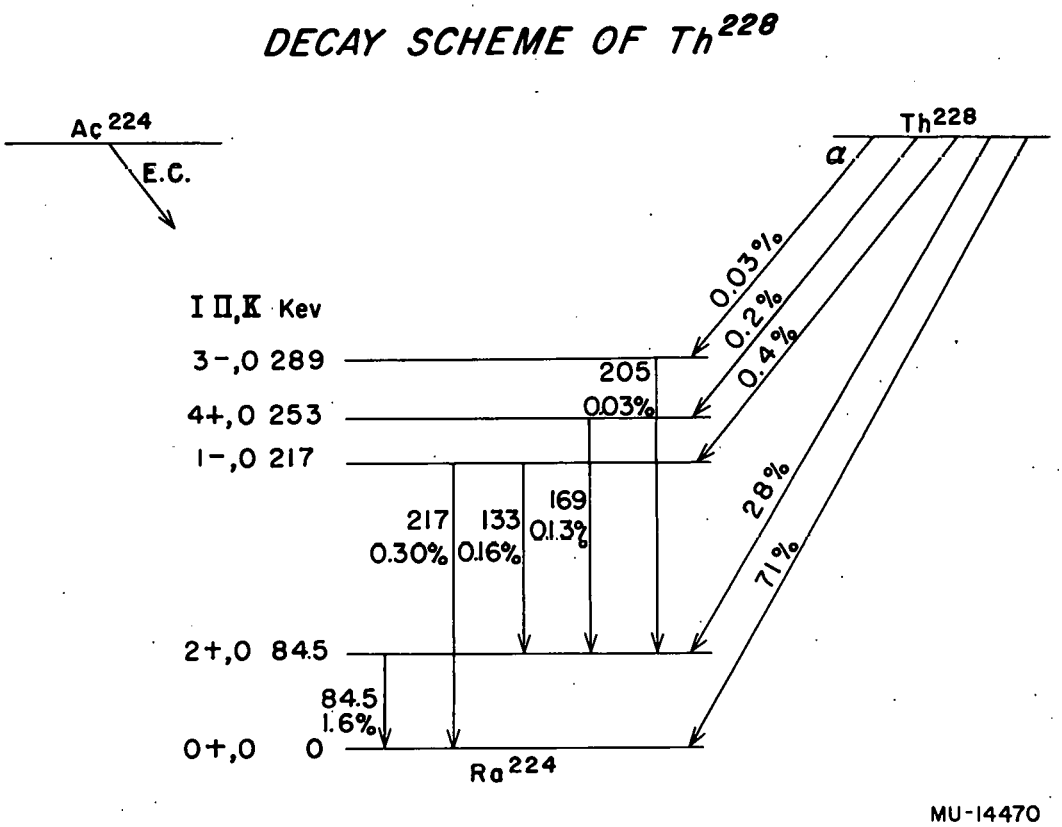

Fig. 33. Decay scheme of Th^{228}.

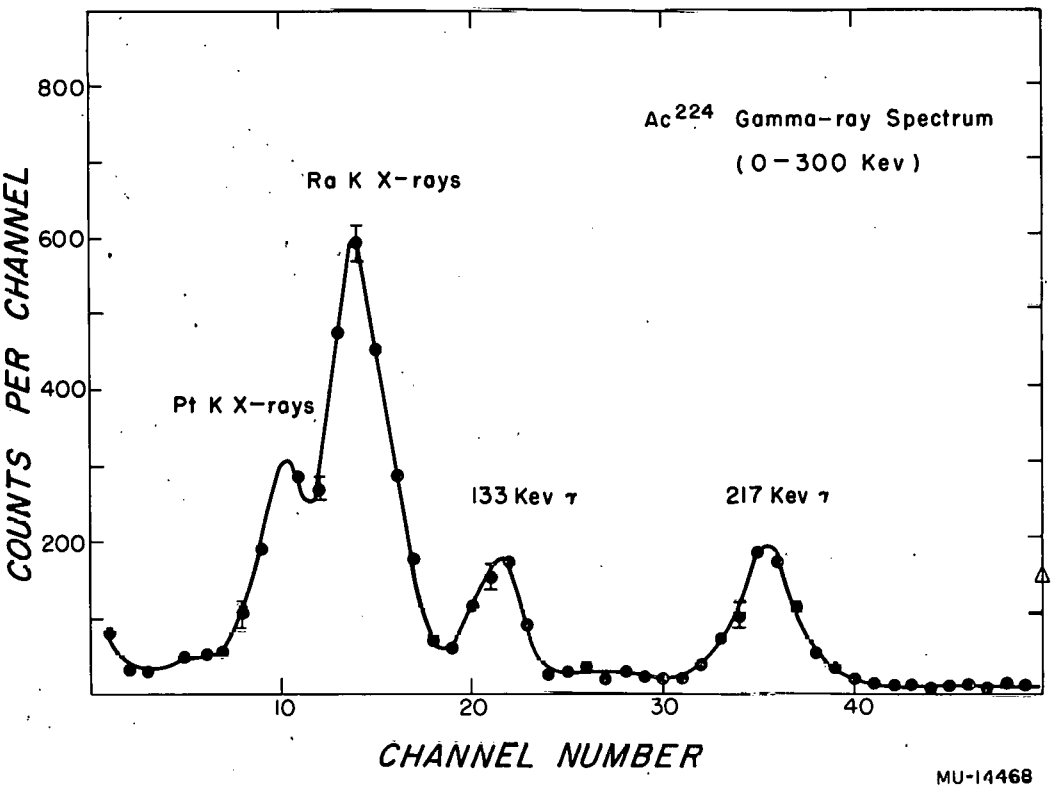

Fig. 34. Gamma-ray spectrum of Ac^{224}, 0 to 300 kev.

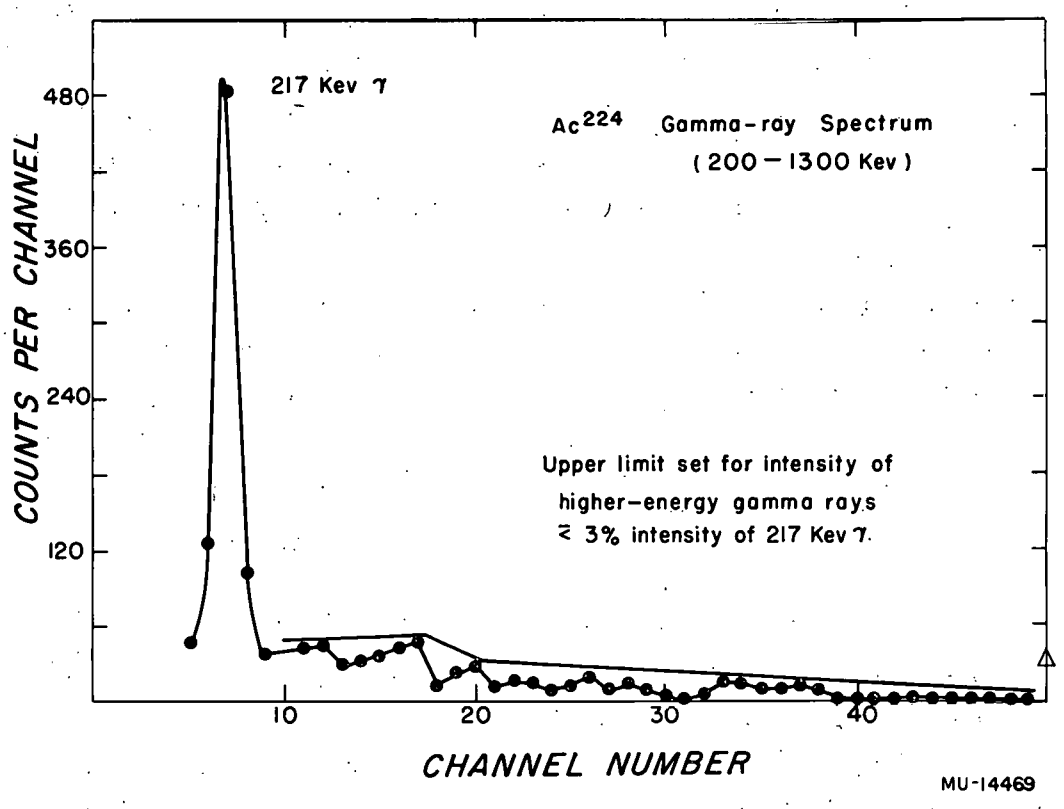

Fig. 35. High-energy gamma-ray spectrum of Ac^{224}.

radium K x-rays are due mainly to K-electron capture, with a slight contribution from the K-conversion of the gamma rays. By integrating the three peaks and making the necessary corrections for counting efficiency, escape-peak loss, and background radiations, one may compare their intensities and calculate the fraction of events populating the 1- state. Making the assumption that the K/L-capture ratio is 4, one obtains a lower limit of 80% for the population to the 1- state.

2. Decay Scheme and Interpretation of Levels

The electron-capture decay scheme of Ac^{224} is shown in Fig. 36. It is seen to be very similar to the electron-capture and beta decay schemes of Ac^{226},[46] with the 1- state being populated in each case.

The levels of Ra^{224} have been interpreted by Stephens,[51] who made the 1- assignment on the basis of conversion-coefficient data, as well as unambiguous alpha-gamma angular-correlation data. However, his reduced transition-probability ratio obtained by removing the third-power energy dependence of the two E1 transitions had rather large limits of error, being 0.36 ± 0.15.[52] Theoretically, this ratio is given by

$$\frac{B_{1 \to 0}}{B_{1 \to 2}} = \frac{(11K_i - K_i|1100)^2}{(11K_i - K_i|1120)^2} = \begin{matrix} 2.00 \text{ for } K_i = 1 \\ 0.50 \text{ for } K_i = 0 \end{matrix}$$

The value obtained from this work is $2.24\ (133/217)^3 = 0.51 \pm 0.05$. This clearly indicates K = 0 for this state, as well as for the even-parity members of the ground-state rotational band.

The log (ft) value for this transition is calculated to be 5.9, which could be allowed or first-forbidden, permitting a spin change of 0 or 1, with or without a change of parity. Since the decay is predominantly to the 1- state with less than 20% to the 0+ and (or) 2+ states, a choice of odd parity would be favored for Ac^{224}. The spin should be less than 2, since the 3- and 4+ states are not populated. The best choice would be 0- or 1-. Stephens favors 0- for Ac^{226}.[53]

Using the Nilsson assignments for the proton and neutron states available, the Moszkowski treatment fails to predict either of these selections.

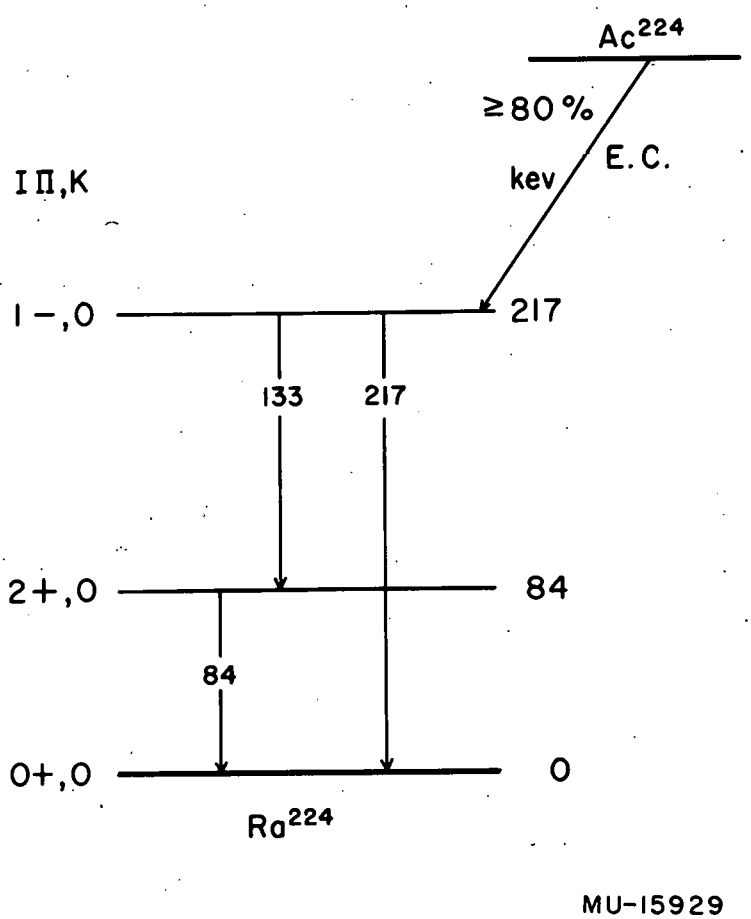

Fig. 36. Electron-capture decay scheme of Ac^{224}.

K. Alpha Decay of Ac^{223}

Ac^{223} was found by Meinke to decay 99% by alpha-particle emission and 1% by electron capture. Its half life was found to be 2.2 min, and its alpha-particle energy was measured as 6.64 Mev.[17] Since its alpha fine structure had never been examined it was felt advisable to investigate it, especially since it is in equilibrium with Pa^{227} and its alpha energy is only slightly larger.

1. Alpha Spectrum

The alpha spectrum of Ac^{223} was obtained on the same plates as that of Pa^{227}. However, since the Pa^{227} alpha groups were focussed in the center of the plate, those of Ac^{223} fell toward the end of the plate and were somewhat distorted. The spectrum obtained is shown in Fig. 37, and the results obtained from two such spectra are summarized in Table XXVI. The excited-state energies should be good to ± 0.7 kev and the abundances to 5%.

Table XXVI. Alpha groups of Ac^{223}

Alpha-particle energy (Mev)[a]	Excited-state energy (kev)	Abundance (%)	Hindrance factor
6.657	0	40.0	1.3
6.643	14.7	46.0	1.0
6.561	98.2	14.0	1.5

[a] Relative to $Bi^{211}_{\alpha_o}$ = 6.620 Mev.

2. Decay Scheme

The alpha-decay scheme of Ac^{223} is shown in Fig. 38. Since no studies were made of the internal transitions, only the energies and populations of the levels are shown. Nothing can be said about the spins and parities of the states at present.

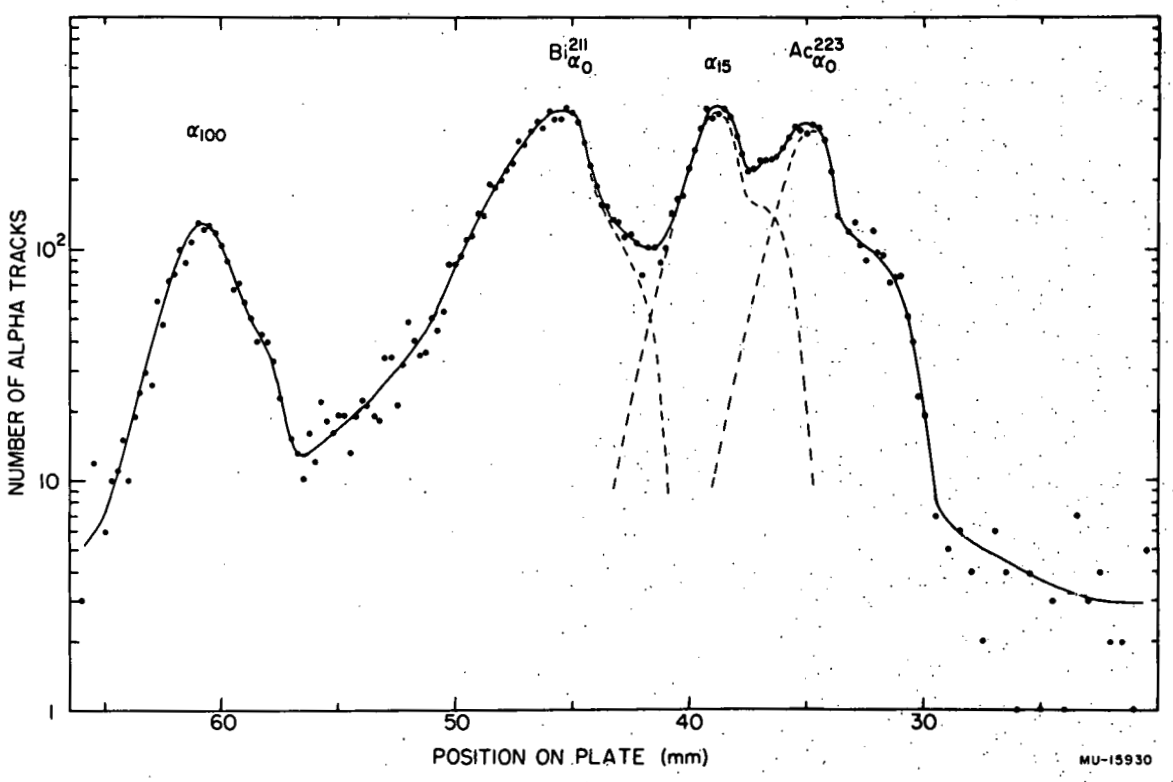

Fig. 37. Alpha-particle spectrum of Ac^{223}—double-focusing spectrograph.

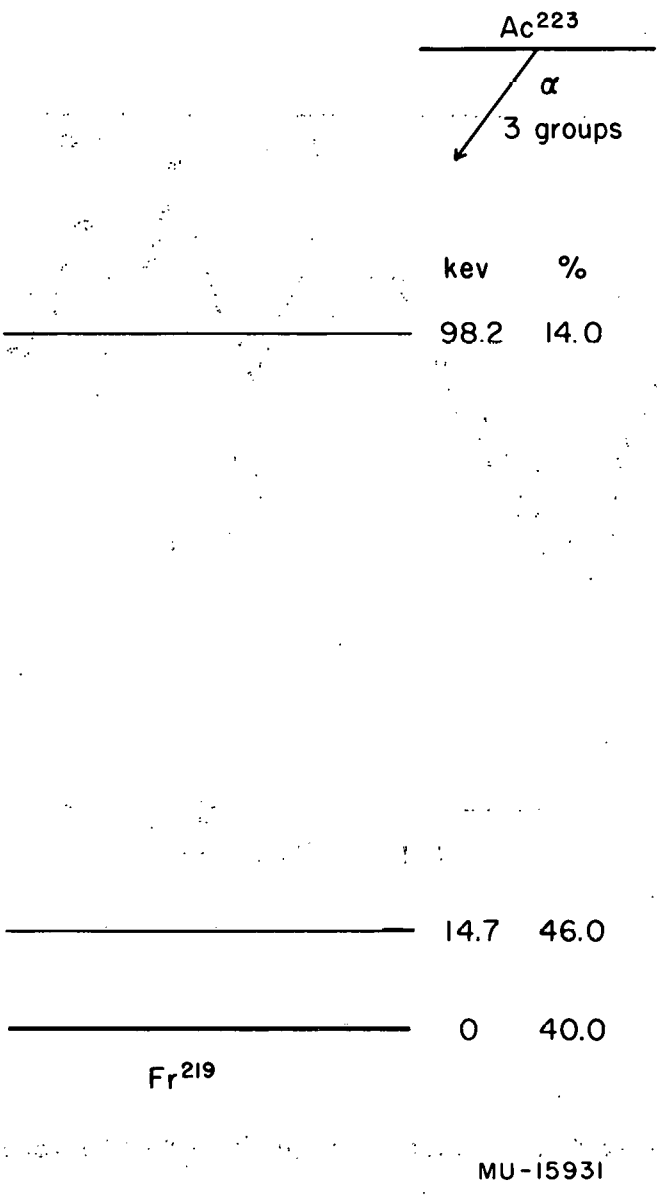

Fig. 38. Alpha decay scheme of Ac^{223}.

IV. CONCLUSION

The fundamental purpose of this study was to provide new information and a better understanding of nuclides lying on the fringe of the collective-model region, with primary emphasis placed on the application of high-resolution alpha spectroscopy to obtain these goals. The results clearly indicate that although the spectra are complex and not fully understood, the collective model still finds useful application in most cases. This model is especially useful in explaining the level structure of even-even nuclides, and is finding wider and wider application to the spectra of odd-mass nuclides, as evidenced by its applicability to the levels populated in Pa^{227} and Pa^{229} alpha decay. Its usefulness in interpreting the levels of odd-odd nuclides remains to be tested as more experimental data accumulate. The alpha decay of Pa^{228} with its extremely complex spectrum stresses the need for even higher resolution and greater sensitivity than is provided by present spectroscopic techniques. Many questions remain unanswered in this region, and it is hoped that improved methods will help to explain these mysteries.

V. ACKNOWLEDGMENTS

Thanks are extended to the United States Atomic Energy Commission and the Radiation Laboratory of the University of California for the facilities and support required for this study, and to the Department of Chemistry and Graduate Division of the University for personal support in the form of scholarships and fellowships.

Helpful comments and suggestions from members of the scientific staff at the Laboratory, including Drs. John O. Rasmussen, Earl K. Hyde, and Glenn T. Seaborg, have been greatly appreciated. Special thanks are extended to Dr. Frank S. Stephens, Jr. for his suggestions and assistance with the scintillation spectrometry, and to Dr. Jack M. Hollander for his help with the electron spectrography.

Grateful recognition is accorded Mrs. Helen Michel, Miss Jill Overstreet, Miss Mary Richardson, and Miss Jacqueline Chang for their help in the tedious and time-consuming task of alpha-track counting. Also appreciated were the efforts of the service staffs of the Laboratory for providing and maintaining equipment, the Health Chemistry Staff for supervision and guidance in handling radioactive materials, the crews of the 60- and 184-inch cyclotrons for their assistance and cooperation in making the bombardments, and the secretarial staff for their assistance throughout the study. Special acknowledgment is accorded my wife, Donna, who in addition to typing this manuscript, has been a constant source of inspiration and encouragement.

The greatest measure of appreciation must go to Dr. Frank Asaro, who capably and unselfishly supervised this study, and to Professor Isadore Perlman, under whose direction it was undertaken and conducted.

VI. REFERENCES

1. M. Goeppert-Mayer, Phys. Rev. 75, 1969 (1949).

2. O. Haxel, J. H. D. Jensen, and H. E. Suess, Phys. Rev. 75, 1766 (1949).

3. A. Bohr and B. R. Mottelson, Kgl. Danske Videnskab. Selskab, Mat.-fys. Medd. 27, No. 16 (1949).

4. M. H. L. Pryce, Proc, Phys. Soc. (London) A65, 773 (1952); D. E. Alburger and M. H. L. Pryce, Phys. Rev. 95, 1482 (1954).

5. W. W. True, Phys. Rev. 101, 1342 (1956); W. W. True and K. W. Ford, Phys. Rev. 109, 1675 (1958).

6. G. Goldhaber and J. Weneser, Phys. Rev. 98, 212 (1955).

7. L. Wilets and M. Jean, Phys. Rev 102, 788 (1956).

8. Richard C. Pilger, Nuclear Decay Schemes in the Actinium Family (Thesis), UCRL-3877, July 1957.

9. Frank Asaro, The Complex Alpha Spectra of the Heavy Elements (Thesis), UCRL-2180, June 1953; F. L. Reynolds, Rev. Sci. Instr. 22, 749 (1951); Asaro, Reynolds, and Perlman, Phys. Rev. 87, 277 (1952).

10. Frank Asaro, UCRL unpublished data (1958).

11. W. G. Smith and J. M. Hollander, Phys. Rev. 101, 746 (1956).

12. Peter Axel, Escape Peak Correction to Gamma-Ray Intensity Measurements Made With Sodium Iodide Crystals, BNL-271, Sept. 1953.

13. M. I. Kalkstein and Jack M. Hollander, A Survey of Counting Efficiencies for a 1-1/2 in.-Diameter x 1-in.-High Sodium Iodide (Thallium Activated) Crystal, UCRL-2764, Oct. 1954.

14. Frank S. Stephens, Jr., Decay Schemes and Nuclear Spectroscopic States in the Heavy Element Region (Thesis) UCRL-2790, June 1955.

15. Donald Strominger, I. Experimental Study of Nuclear Isomers in the Millimicrosecond Lifetime Range; II. Application of Nilsson's Wave Functions for Deformed Nuclei (Thesis) UCRL-3374, June 1956.

16. Earl K. Hyde, in Proc. Intl. Conf. Peaceful Uses Atomic Energy, Geneva, 1955, Vol. 7, p. 281.

17. W. Wayne Meinke, High-Energy Bombardment Products of Thorium (Thesis), UCRL-483, Nov. 1949.

18. Ong Ping Hok, The Beta Decay of Protactinium Isotopes (Thesis), The Free University of Amsterdam, 1955.

19. K. A. Kraus and F. Nelson, Proc. Intl. Conf. Peaceful Uses Atomic Energy, Geneva, 1955, Vol. 7, p. 113; E. H. Huffman, G. M. Iddings, and R. C. Lilly, J. Am. Chem. Soc. 73, 4474 (1951).

20. K. A. Kraus and G. E. Moore, J. Am. Chem. Soc. 73, 9 (1951); 73, 2900 (1951).

21. J. Golden and A. G. Maddock, J. Inorg. and Nucl. Chem. 2, 1, 46 (1956).

22. D. I. Katzin, Proc. Intl. Conf. Peaceful Uses Atomic Energy, Geneva, 1955, Vol. 7, p. 407.

23. E. K. Hyde, M. H. Studier, and R. J. Bruelman, reported in Argonne National Laboratory Report ANL-4112 (1948).

24. W. W. Meinke, A. Ghiorso, and G. T. Seaborg, Phys. Rev. 81, 782 (1951).

25. L. M. Slater and G. T. Seaborg, unpublished data (1951). Reported in Ref. 46.

26. I. Perlman and J. O. Rasmussen, in Handbuch der Physik (Springer-Verlag, Berlin, 1957) Vol. 42, p. 109; Alpha Radioactivity, UCRL-3424 June 1956.

27. M. E. Rose, Internal Conversion Coefficients, in Beta- and Gamma Spectroscopy, K. Siegbahn, ed. (Interscience, New York, 1955).

28. F. S. Stephens, Jr., Phys. Rev. 98, 262 A (1955).

29. A. Bohr, P. O. Froman, and B. R. Mottelson, Kgl. Danske Videnskab Selskab. Mat.-fys. Medd. 29, No. 10 (1955).

30. S. G. Nilsson, Kgl. Danske Videnskab Selskab. Mat.-fys. Medd. 29, No. 16 (1955).

31. F. S. Stephens, Jr., F. Asaro, and I. Perlman, Phys. Rev. (to be published, 1958).

32. P. O. Froman, Kgl. Danske Videnskab Selskab. Mat.-fys. Skr. 1, No. 3 (1957).

33. D. Strominger and J. O. Rasmussen, Nuclear Phys. 3, 197 (1957).

34. L. L. Goldin, G. I. Novikova, and E. F. Tretyakov, Phys. Rev. 103, 1004 (1956).

35. J. O. Newton, Nuclear Phys. 5, 218 (1958).

36. John P. Hummel, Alpha-Decay Studies in the Heavy-Element Region (Thesis), UCRL-3456, July 1956.

37. Thomas O. Passell, Internal Conversion of Gamma Radiation in the L Subshells (Thesis), UCRL-2528, March 1954.

38. Ong Ping Hok and E. Arbman, Arkiv. Fysik 11, 193 (1956).

39. I. Bergstrom and R. D. Hill, Arkiv. Fysik 8, 21 (1954).

40. H. C. Box and G. S. Klaiber, Phys. Rev. 95, 1247 (1954).

41. S. Bjornholm, O. Nathan, O. B. Nielsen, and R. K. Sheline, Nuclear Phys. 4, 313 (1957).

42. S. A. Moszkowski, oral report, UCRL Nuclear Spectroscopy Seminar (1958).

43. M. H. Studier and R. J. Bruehlman, ANL-4252 (1949).

44. M. H. Studier and E. K. Hyde, Phys. Rev. 74, 591 (1948).

45. Ong Ping Hok, P. Kramer, G. Meijer, J. W. R. Fennema, and W. L. Zijp, Physica 21, 719 (1955).

46. D. Strominger, J. M. Hollander, and G. T. Seaborg, Rev. Mod. Phys. 30, No. 2, Part II, 585 (1958).

47. F. S. Stephens, Jr., unpublished data (1957).

48. Ong Ping Hok and G. J. Sizoo, Physica 20, 77 (1954).

49. C. I. Browne, D. C. Hoffman, H. L. Smith, M. E. Bunker, J. P. Mize, J. W. Starner, R. L. Moore, and J. P. Balagna, Phys. Rev. 96, 827 A (1954).

50. W. D. Brodie, Proc. Phys. Soc. (London) 67 A, 265 (1954).

51. F. S. Stephens, Jr., F. Asaro, and I. Perlman, Phys. Rev. 107, 1091 (1957).

52. F. S. Stephens, Jr., F. Asaro, and I. Perlman, Phys. Rev. 100, 1543 (1955).

53. F. S. Stephens, Jr., F. Asaro, and I. Perlman, to be published (1958).